



## Dynamical analysis of toxin-producing *Microcystis aeruginosa* aggregation on filter-feeding fish in aquatic ecosystem

Parvez Akhtar<sup>a</sup>, Souvick Karmakar<sup>a</sup>, Nirmalya Mondal<sup>a</sup>, Guruprasad Samanta<sup>a,\*</sup>

<sup>a</sup>Department of Mathematics, Indian Institute of Engineering Science and Technology, Shibpur, Howrah - 711103, India

**Abstract.** The predator-prey interaction in mathematical ecology is a basic phenomenon in nature that has an important impact on community organization and on preserving the ecological diversity. In this research work, we have developed a unique aquatic ecological model to investigate the interaction between *Microcystis aeruginosa* and filter-feeding fish in presence of toxicity. This model specifically focuses on describing the phenomenon of *Microcystis aeruginosa* aggregation and the effect of toxin producing *Microcystis aeruginosa* blooms on filter-feeding fishes. Holling type II and Holling type III functional responses are used in our proposed model. Here, we have analyzed the model parameters to examine the stability of all equilibrium points in our system. Our system shows local bifurcations, including transcritical, saddle-node, Hopf, generalized Hopf, Cusp bifurcation and Bogdanov-Takens. Further, we have seen global bifurcation, particularly homoclinic bifurcation. Additionally, we have provided evidence of the hysteresis phenomena and basins of attraction to support the existence of bi-stability. Multiple numerical examples support each of these theoretical findings.

### 1. Introduction

Algal blooms are one of the major environmental global problems throughout the world these days. Blooms, which are sudden large concentrations of algal growth in the aquatic system that discolor water from its normal form. These algal blooms can deplete the oxygen of surrounding water, which is harmful to fish and other aquatic life. In addition, certain algae species can produce toxins harmful to humans and animals. Hence, the drastically resultant effects of algal blooms might have a severe impact on the natural growth of aquatic ecosystems. As a result, control and removal of algal blooms are imperative globally. The most common method to remove algal blooms is the use of filter-feeding fish to control algae, which had worked well in healing the biological community and giving out good response. It minimizes the amount of algae present, ensures that the water quality remains transparent, and enhances biodiversity [2].

---

2020 *Mathematics Subject Classification.* Primary 92B05; Secondary 92D25, 92D40.

*Keywords.* Local bifurcation; Aggregation; Basins of attraction; Hysteresis; Toxicity.

Received: 24 December 2024; Accepted: 25 December 2024

Communicated by Maria Alessandra Ragusa

Research supported by Indian Institute of Engineering Science and Technology, Shibpur

\* Corresponding author: Guruprasad Samanta

*Email addresses:* pakhtardream@gmail.com (Parvez Akhtar), skarmakaruttarpara@gmail.com (Souvick Karmakar), nirmalyamonda197@gmail.com (Nirmalya Mondal), g\_p\_samanta@yahoo.co.uk, gpsamanta@math.iiests.ac.in (Guruprasad Samanta)

ORCID iDs: <https://orcid.org/0009-0006-5924-4319> (Parvez Akhtar), <https://orcid.org/0009-0003-2256-9652> (Souvick Karmakar), <https://orcid.org/0009-0009-4400-2829> (Nirmalya Mondal), <https://orcid.org/0000-0002-2956-6265> (Guruprasad Samanta)

Algal blooms are rapid and extensive growths of algae in aquatic systems, which might lead to an overabundance of nutrients such as nitrogen and phosphorus. These blooms can utilize the oxygen in the water that aquatic animals need to survive, creating dead zones. There may be internal and external reasons for algal blooms. The causes of algal blooms are usually associated with external factors such as agricultural runoff, wastewater discharge and climate changes or also internal factors including migration and aggregation of algae population [3]. Algal aggregation can happen in two main ways. The first is when individual cells get together to form gel colonies. The second being efficient grouping of daughter cells by single cell division and growth. Meanwhile, algae population can slowly increase, promote vertical movement and rise to water surface to form algal aggregations leading to the generation of algal blooms simultaneously.

In the sphere of environmental science, along with aquatic biology, there have been numerous researchers working on how the reproduction of aquatic life is impacted by algae growth over the last ten years [4, 5, 7, 8]. Following the process of aggregation, *Microcystis aeruginosa* forms a dense gel-like coating that is hard to digest by filter-feeding fish. When microcystis cells aggregate, they can produce more algal toxins than their individual cells, which reduces the danger of being eaten. On the other hand, there exists a food web in aquatic environments, where some fish consume algae and predatory fish consume smaller fish (prey) [9].

The mathematical model of ecological communities and population dynamics research technique is a complete approach that combines coordination, order and purpose. This method forms the basis for studying biological systems via trophic level analysis, system viewpoint, with dynamic analysis. The primary objective of modeling population dynamics is to enhance understanding of the interactions between populations and how they depend on internal and external circumstances [10, 11]. Predator-prey interaction models have been extensively studied in recent decades to understand the dynamics of various species and their impact on real-life situations [1, 6, 18]. However, in recent decades, there has been a growing focus and fast development of the complete study approach of ecological model and population dynamics, particularly in the field of bifurcation dynamics. Mukherjee and Maji [12] examined the dynamics of bifurcation of a predator-prey model. Prey refuge is an important factor for occurrence of bifurcation, namely Hopf, saddle-node, transcritical and Bogdanov-Takens bifurcations. The underlying conditions have been established and these results are useful and essential. Another work on prey refuge was discussed using strong Allee effect and Michaelis–Menten predator–prey model [19].

In addition to this, numerous other studies have made advancements in the areas of population dynamics and ecological models [13–17, 20–22, 24, 28]. The field of modeling and population dynamics has seen a considerable progress leading to the discovery of numerous important research findings. Unfortunately, progress in the development of models has been relatively sluggish especially regarding research on the impact of algal aggregation.

Our primary claim in this paper is: filter-feeding fish are capable of effectively managing *Microcystis aeruginosa* blooms in subtropical lake reservoirs. The aggregation of *Microcystis aeruginosa* is advantageous in reducing the danger of predation and provides a certain level of self-protection. Additionally, *Microcystis aeruginosa* blooms produce toxic elements which affect the growth of filter-feeding fish population. Furthermore, in section 2, we have introduced an aquatic ecological model to explain the process of *Microcystis aeruginosa* aggregation and its impact on the feeding dynamics of filter-feeding fish. In section 3 we have shown the positivity of the solution of the proposed model. The prey-predator model's positivity ensures that populations have a real and meaningful impact. Next the 4<sup>th</sup> section contains the existence criteria of equilibrium points of system (2.1). A thorough study of the stability of the equilibrium points of our system has been presented in section 5. We have performed a theoretical study in section 6, that enables us to determine the critical threshold condition by identifying one parametric bifurcation such as transcritical bifurcation, saddle-node bifurcation, Hopf-bifurcation. The two-parametric bifurcations such as Bogdanov-Takens bifurcation, generalized Hopf-bifurcation and Cusp bifurcation have also been exhibited. Section 7 presents numerical simulation of our model. It provides a thorough explanation and examination of bifurcations with one and two parameters, including a discussion on the system's basins of attraction and hysteresis. This section also includes a global bifurcation, i.e., Homoclinic bifurcation. At last, in section 8 we have given the discussion of our work.

## 2. Model Formulation

To develop a new aquatic ecological model including the effects of aggregation and toxicity, we have taken some modeling assumptions that are presented as follows:

*Microcystis aeruginosa*, a type of cyanobacteria often seen in freshwater environments, can engage in interactions with filter-feeding fish within a confined aquatic ecosystem. In proposed system (2.1) the variables  $x(t)$  and  $y(t)$  represent the population sizes of *Microcystis aeruginosa* (prey) and filter-feeding fish (predator) respectively, at a given time  $t$ . The parameter  $r_1$  signifies the intrinsic growth rate of *Microcystis aeruginosa* while its maximum sustainable size or carrying capacity is denoted by  $K$ . Filter-feeding fish possesses specialized anatomical features such as gill rakers or modified gill arches, which enable them to strain planktons and small organisms from the water as they move. *Microcystis aeruginosa*, being a type of cyanobacteria commonly found in freshwater habitats, has the potential to form blooms of cyanobacteria.

- In our proposed model (2.1),  $r_1x\left(1 - \frac{x}{K}\right)$  is the growth function of *Microcystis aeruginosa*. Here  $r_1$  represents the intrinsic growth rate and  $K$  is the maximum carrying capacity of the environment.
- The mathematical function  $\frac{\beta(x-g)y}{B+x-g}$  describes the consumption rate of filter-feeding fish with grazing coefficient  $\beta$ , *Microcystis aeruginosa* aggregation coefficient is denoted as  $g$  and half saturation constant as  $B$ . The aggregation of *Microcystis aeruginosa* serves as a strong defense mechanism against filter-feeding fish grazing, making it a viable self-protection strategy. Here, if *Microcystis aeruginosa* does not gather together then the parameter  $g$  vanishes, but if they aggregate more and more, then  $g$  tends to  $x(t)$ .
- The aggregation of *Microcystis aeruginosa* often includes an extensive number of cells, resulting in an enormous mass which makes it unsuitable for filter-feeding fish grazing. Consequently, filter-feeding fishes are limited to grazing on *Microcystis aeruginosa* monomer. So, we may say that the quantity of *Microcystis aeruginosa* aggregation and *Microcystis aeruginosa* monomer is the primary factor that determines the growth of filter-feeding fish. Here in our model (2.1), the function  $\frac{\gamma\beta(x-g)y}{B+x-g}$  describes how the aggregation affects the filter-feeding fishes to consume those aggregated *Microcystis aeruginosa*, where  $\gamma$  is the coefficient of consumption rate of filter-feeding fish. Next the mathematical function  $r_2y\left(1 - \frac{x}{K}\right)$  is used to describe the impact of *Microcystis aeruginosa* monomer on filter-feeding fish abundance. Here  $r_2$  is the intrinsic growth rate of filter-feeding fish due to *Microcystis aeruginosa* monomer.
- We have used the function  $d_1y$  as the natural mortality rate of filter-feeding fish, with  $d_1$  as natural mortality coefficient.
- Lastly, we have introduced toxicity, and the toxicity has been defined as function  $\frac{cx^2y^2}{A+x^2}$ , where  $c$  is the toxicity parameter and  $\sqrt{A}$  is half-saturation constant. According to the scientific design of the experiment, it is presumed that toxic substances occur in *Microcystis aeruginosa*, or they serve as producers of the toxin. Consequently, anything that filter-feeding fishes use as food to feed or nourish themselves, like *Microcystis aeruginosa*, shall make the fishes fall ill or give rise to diseases and bring about their death.

The proposed model is as follows:

Table 1: List of parameters with their biological meaning

Parameters	Descriptions of Parameters
$x(t)$	Population size of <i>Microcystis aeruginosa</i> (prey) at time $t$
$y(t)$	Population size of filter-feeding fish (predator) at time $t$
$r_1$	Intrinsic growth rate of <i>Microcystis aeruginosa</i> (prey) ( $> 0$ )
$K$	Carrying capacity of the environment ( $> 0$ )
$\beta$	Grazing coefficient of filter-feeding fish
$g$	Coefficient of <i>Microcystis aeruginosa</i> aggregation
$B$	Half saturation constant
$\gamma$	Absorption coefficient of filter-feeding fish
$r_2$	Intrinsic growth rate of filter-feeding fish (predator) ( $> 0$ )
$d_1$	Natural mortality rate of predator species
$\eta_1$	Toxicity coefficient of predator population
$A$	Square of the half saturation constant

$$\begin{aligned} \frac{dx}{dt} &= r_1x\left(1 - \frac{x}{K}\right) - \frac{\beta(x-g)y}{B+x-g} \equiv F(x,y), \text{ (say)} \\ \frac{dy}{dt} &= \frac{\gamma\beta(x-g)y}{B+x-g} + r_2y\left(1 - \frac{x}{K}\right) - d_1y - \frac{\eta_1x^2y^2}{A+x^2} \equiv G(x,y) = yf_2(x,y), \text{ (say)} \end{aligned} \tag{2.1}$$

With  $x(0) > 0$  and  $y(0) > 0$ , it is assumed that  $B > g$ .

All the parameters and their respective biological meanings are mentioned in Table 1 :

### 3. Positivity and Boundedness

Positivity of solutions of a prey-predator model ensures that the model is biologically meaningful. In this context we have the following theorem.

**Theorem 3.1.** Each solution of (2.1) remains positive for any  $x(0) > 0, y(0) > 0; \forall t > 0$ .

*Proof.*

$$\frac{dy}{dt} = yf_2(x,y) \tag{3.1}$$

where,  $f_2(x,y) = \frac{\gamma\beta(x-g)}{B+x-g} + r_2\left(1 - \frac{x}{K}\right) - d_1 - \frac{\eta_1x^2y}{A+x^2}$ .

Now from equation (3.1) we get,

$$y(t) = y(0) \exp\left(\int_0^t f_2(x,y)dt\right) > 0, \text{ for } y(0) > 0.$$

Thus,  $y(t) > 0$  whenever  $y(0) > 0, \forall t > 0$ .

Now we have to prove  $x(t) > 0, \forall t > 0$ .

To show the positivity of  $x(t)$  in system (2.1), firstly we claim that  $x(t) > 0, \forall t \in [0, k]$ , where  $0 < k \leq \infty$ . Now let us take that our assumption is incorrect. Then,  $\exists t_1 \in (0, k)$  s.t  $x(t_1) = 0$  and  $x(t) > 0 \forall t \in [0, t_1)$  and  $\dot{x}(t_1) \leq 0$ .

From 1<sup>st</sup> equation of system (2.1) we get,

$$\left[ \frac{dx}{dt} \right]_{t=t_1} = r_1 x(t_1) \left( 1 - \frac{x(t_1)}{K} \right) - \frac{\beta(x(t_1) - g)y(t_1)}{B + x(t_1) - g}$$

Now, as  $x(t_1) = 0$ , so,

$$\left[ \frac{dx}{dt} \right]_{t=t_1} = \frac{\beta g y(t_1)}{B - g} > 0, \text{ as } B > g \text{ and } y(t_1) > 0.$$

Therefore, we arrive a contradiction and hence  $x(t_1) > 0, \forall t > 0$ .  $\square$

**Theorem 3.2.** Every solution of system (2.1) is uniformly bounded in  $\mathbb{R}_+^2$  whenever  $d_1 > r_2$ .

*Proof.* Now let us assume,  $w(t) = x(t) + \frac{y(t)}{\gamma}$ . So we have,

$$\begin{aligned} \frac{dw}{dt} &= \frac{dx}{dt} + \frac{1}{\gamma} \frac{dy}{dt} \\ \implies \frac{dw}{dt} &= r_1 x \left( 1 - \frac{x}{K} \right) + \frac{r_2}{\gamma} y \left( 1 - \frac{x}{K} \right) - \frac{d_1}{\gamma} y - \frac{\eta_1 x^2 y^2}{\gamma(A + x^2)} \\ &\leq (r_1 + 1)x - \frac{r_1 x^2}{K} + \frac{1}{\gamma} (r_2 - d_1)y - x \\ &= -\frac{r_1}{K} \left\{ x - \frac{K}{2r_1} (r_1 + 1) \right\}^2 + \frac{K}{4r_1} (r_1 + 1)^2 - \left\{ x + \frac{1}{\gamma} (d_1 - r_2)y \right\} \\ &\leq \frac{K(r_1 + 1)^2}{4r_1} - \left[ x + \frac{1}{\gamma} (d_1 - r_2)y \right] \\ \implies \frac{dw}{dt} &\leq M - \mu w, \text{ where, } M = \frac{K(r_1 + 1)^2}{4r_1} \text{ and } \mu = \text{Min}\{1, d_1 - r_2\}, \text{ since } d_1 > r_2 \\ \implies \frac{dw}{dt} + \mu w &\leq M \end{aligned}$$

Now by the principle of differential inequality, we get,  $0 < w(t) \leq \frac{M}{\mu} (1 - e^{-\mu t}) + w(0)e^{-\mu t}$ . As  $t \rightarrow \infty$ ,

we get  $0 < w(t) \leq \frac{M}{\mu} + \epsilon$ , for any  $\epsilon > 0$ . Hence, any solution of system (2.1) in  $\mathbb{R}_+^2$  enter in the region:

$\Omega = \left\{ (x, y) \in \mathbb{R}_+^2 : 0 < x(t) + \frac{y(t)}{\gamma} \leq \frac{M}{\mu} + \epsilon, \text{ for } \epsilon > 0, d_1 > r_2 \right\}$ . So, every solution of system (2.1) is uniformly bounded.

$\square$

## 4. Equilibrium Points

### 4.1. Trivial and Axial equilibrium

System (2.1) possesses a trivial equilibrium point, denoted by  $E_0(0, 0)$ , and one axial equilibrium point, denoted by  $E_a(K, 0)$ .

#### 4.2. Interior Equilibrium

Solving two non-trivial nullclines of system (2.1) yields the interior equilibrium point,

$$f_2(x, y) = \frac{\gamma\beta(x - g)}{B + x - g} + r_2 \left(1 - \frac{x}{K}\right) - d_1 - \frac{\eta_1 x^2 y}{A + x^2} = 0$$

$$\implies y = \frac{A + x^2}{\eta_1 x^2} \left( \frac{\gamma\beta(x - g)}{B + x - g} + r_2 \left(1 - \frac{x}{K}\right) - d_1 \right). \tag{4.1}$$

$$F(x, y) = r_1 x \left(1 - \frac{x}{K}\right) - \frac{\beta(x - g)y}{B + x - g} = 0 \tag{4.2}$$

If we now take the value of  $y$  from equation (4.1) and substitute it into equation (4.2), we get the following:  $\phi(x) \equiv a_6 x^6 + a_5 x^5 + a_4 x^4 + a_3 x^3 + a_2 x^2 + a_1 x + a_0 = 0$ , where

$$a_0 = A\beta g K [(g - B)(r_2 - d_1) + \gamma\beta g]$$

$$a_1 = -\beta A [K(B(d_1 - r_2) + g(2\beta\gamma - 2d_1 + 2r_2)) - gr_2(B - g)]$$

$$a_2 = \beta \left[ -d_1 K(A + g(g - B)) + r_2(A(-B + 2g + K) + gK(g - B)) + \gamma\beta K(A + g^2) \right]$$

$$a_3 = \beta r_2 [B(g + K) - g(g + 2K) - A] - \beta d_1 K(B - 2g) - \eta_1 K r_1 (B - g)^2 - 2\beta^2 \gamma g K$$

$$a_4 = \beta r_2 (2g + K - B) + \eta_1 r_1 (B - g)(B - g - 2K) + \beta K (\gamma\beta - d_1)$$

$$a_5 = -\eta_1 r_1 [2(g - B) + K] - r_2$$

$$a_6 = \eta_1 r_1$$

Let  $x^*$  be a positive solution of  $\phi(x) = 0$ . From equation (4.1), we have,

$$y = \frac{A + x^{*2}}{\eta_1 x^{*2}} \left( \frac{\gamma\beta(x^* - g)}{B + x^* - g} + r_2 \left(1 - \frac{x^*}{K}\right) - d_1 \right) = y^* \text{ (say) provided, } \frac{\gamma\beta x^*}{B + x^* - g} + r_2 > \frac{r_2 x^*}{K} + \frac{\gamma\beta g}{B + x^* - g} + d_1$$

Thus,  $E_I(x^*, y^*)$  is the interior equilibrium point of system (2.1).

It is observed that by changing specific parameter values, the number of interior equilibrium points of system (2.1) varies accordingly. In Fig.1, we have shown the variations of equilibrium points by changing the parameter value of  $d_1$ . In the following table 2, we have mentioned these equilibrium points with its coordinates and their parameter sets along with their stability behavior.

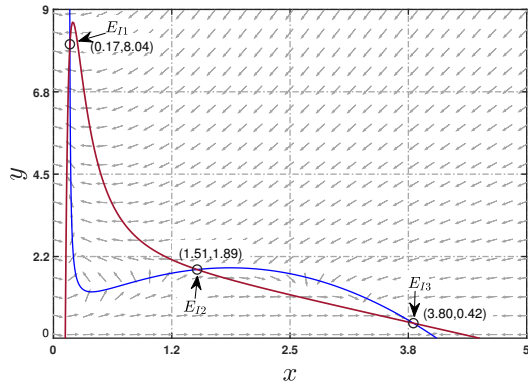
#### 5. Stable behavior

Jacobian matrix of system (2.1) at  $E(x, y)$  is

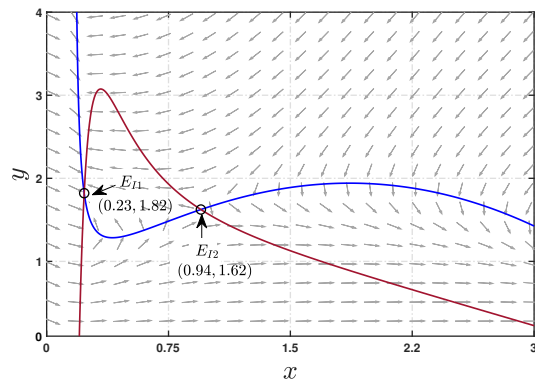
$$J(x, y) = \begin{bmatrix} \frac{\partial F}{\partial x} & \frac{\partial F}{\partial y} \\ \frac{\partial G}{\partial x} & \frac{\partial G}{\partial y} \end{bmatrix}$$

Table 2: **Variation of interior equilibrium points**

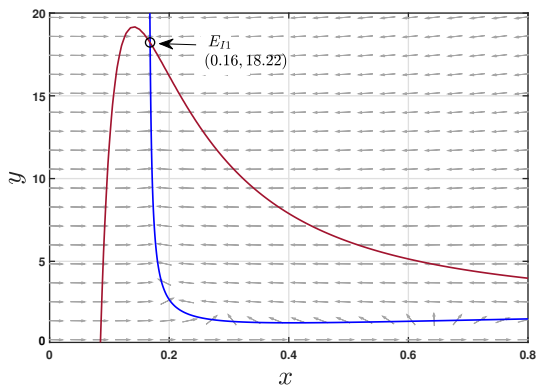
No of Equilibrium points	Parameters set	Equilibrium point co-ordinates	Stability
3	$r_1 = 1.18, K = 4.06, \beta = 0.71, g = 0.164, B = 0.27, \gamma = 0.84, r_2 = 0.61, d_1 = 0.49, \eta_1 = 0.25, A = 0.5$	$E_{I1}(0.17, 8.04)$	Stable
		$E_{I2}(1.51, 1.89)$	Unstable
		$E_{I3}(3.80, 0.42)$	Stable
2	$r_1 = 1.18, K = 4.06, \beta = 0.71, g = 0.164, B = 0.27, \gamma = 0.84, r_2 = 0.61, d_1 = 0.65, \eta_1 = 0.25, A = 0.5$	$E_{I1}(0.23, 1.82)$	Stable
		$E_{I2}(0.94, 1.62)$	Unstable
1	$r_1 = 1.18, K = 4.06, \beta = 0.71, g = 0.164, B = 0.27, \gamma = 0.84, r_2 = 0.61, d_1 = 0.35, \eta_1 = 0.25, A = 0.5$	$E_{I1}(0.16, 18.22)$	Stable
0	$r_1 = 1.18, K = 4.06, \beta = 0.71, g = 0.164, B = 0.27, \gamma = 0.84, r_2 = 0.61, d_1 = 0.85, \eta_1 = 0.25, A = 0.5$	-	-



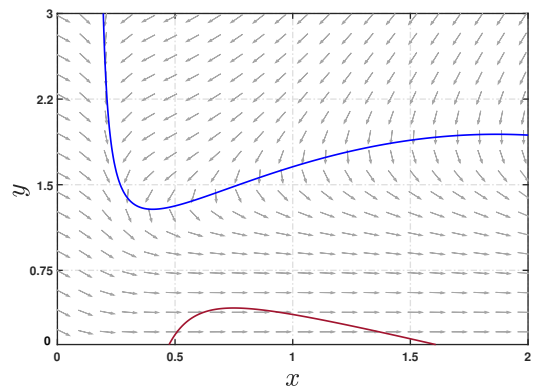
(a) 3 interior equilibrium points



(b) 2 interior equilibrium points



(c) 1 interior equilibrium point



(d) Zero interior equilibrium point

Figure 1: Variation in prey and predator nullcline interior equilibrium points alongwith vector fields with adequate parameter values. The non-trivial  $x$  and  $y$  nullclines are represented by the blue and red curve respectively.

$$= \begin{bmatrix} -\frac{B\beta y}{(B-g+x)^2} + r_1 \left(1 - \frac{2x}{K}\right) & -\frac{\beta(x-g)}{B-g+x} \\ \frac{\beta\gamma y}{(B-g+x)^2} - \frac{2A\eta_1 xy^2}{(A+x^2)^2} - \frac{r_2 y}{K} & \frac{\beta\gamma(x-g)}{B-g+x} - \frac{2\eta_1 x^2 y}{A+x^2} + r_2 \left(1 - \frac{x}{K}\right) - d_1 \end{bmatrix}$$

**Theorem 5.1.** Equilibrium state  $E_0(0, 0)$  is unstable. Moreover, it is a unstable node if  $r_2 > \frac{\beta\gamma g}{B-g} + d_1$  and unstable saddle if  $r_2 < \frac{\beta\gamma g}{B-g} + d_1$ .

*Proof.* At  $E_0(0, 0)$ , Jacobian matrix is obtained as,

$$J(E_0) = \begin{bmatrix} r_1 & \frac{\beta g}{B-g} \\ 0 & -\frac{\beta\gamma g}{B-g} - d_1 + r_2 \end{bmatrix}$$

The eigenvalues of  $J(E_0)$  are  $r_1$  and  $\left(-\frac{\beta\gamma g}{B-g} - d_1 + r_2\right)$ . If  $r_2 > \frac{\beta\gamma g}{B-g} + d_1$ , then both eigenvalue are positive. So,  $E_0(0, 0)$  is a unstable node. On the other hand, if  $r_2 < \frac{\beta\gamma g}{B-g} + d_1$ , then one eigen value is positive and another is negative. Hence,  $E_0(0, 0)$  is a unstable saddle.  $\square$

**Theorem 5.2.** Predator-free equilibrium point  $E_a(K, 0)$  is locally asymptotically stable (LAS) if  $\frac{\beta\gamma(K-g)}{B-g+K} < d_1$  and it is an unstable saddle if  $\frac{\beta\gamma(K-g)}{B-g+K} > d_1$ .

*Proof.* Jacobian matrix  $J(E)$  at  $E_a = (K, 0)$  is,

$$J(E) = \begin{bmatrix} -r_1 & -\frac{\beta(K-g)}{B-g+K} \\ 0 & -d_1 + \frac{\beta\gamma(K-g)}{B-g+K} \end{bmatrix}$$

The eigenvalues of  $J(E)$  are  $-r_1$  and  $\left(-d_1 + \frac{\beta\gamma(K-g)}{B-g+K}\right)$ . Therefore, the predator free equilibrium is locally asymptotically stable (LAS) if  $\frac{\beta\gamma(K-g)}{B-g+K} < d_1$  and it is an unstable saddle if  $\frac{\beta\gamma(K-g)}{B-g+K} > d_1$ .  $\square$

**Theorem 5.3.** The survival of the both species reflects the existence of the interior equilibrium state  $E_I(x^*, y^*)$ , that leads to the following stability behavior of  $E_I(x^*, y^*)$ :

- I. stable node when  $\Gamma < 0, \Delta > 0, \Gamma^2 - 4\Delta \geq 0$
- II. unstable node when  $\Gamma > 0, \Delta > 0, \Gamma^2 - 4\Delta \geq 0$
- III. stable spiral provided  $\Gamma < 0, \Gamma^2 - 4\Delta < 0$
- IV. unstable spiral when  $\Gamma > 0, \Gamma^2 - 4\Delta < 0$
- V. unstable saddle when  $\Delta < 0$
- VI. stable centre provided  $\Gamma = 0, \Delta > 0$

where,  $\Gamma = \text{Tr}(J(x^*, y^*))$  and  $\Delta = \det(J(x^*, y^*))$

*Proof.* At the interior equilibrium point  $E_I(x^*, y^*)$ , the Jacobian matrix is given by,

$$J(E_I) = \begin{bmatrix} \frac{\partial F}{\partial x} & \frac{\partial F}{\partial y} \\ y \frac{\partial f_2}{\partial x} & y \frac{\partial f_2}{\partial y} \end{bmatrix}_{E_I} = \begin{bmatrix} C_{11} & C_{12} \\ C_{21} & C_{22} \end{bmatrix} = C$$

where,

$$\begin{aligned} C_{11} &= -\frac{B\beta y^*}{(B-g+x^*)^2} + r_1 \left(1 - \frac{2x^*}{K}\right) \\ C_{12} &= -\frac{\beta(x^* - g)}{B-g+x^*} \\ C_{21} &= -\frac{2A\eta_1 x^* y^{*2}}{(A+x^{*2})^2} + \frac{By^*\beta\gamma}{(B-g+x^*)^2} - \frac{r_2 y^*}{K} \\ C_{22} &= -\frac{\eta_1 y^* x^{*2}}{A+x^{*2}} \end{aligned}$$

Now, for matrix C, the characteristic equation becomes

$$|A - \lambda I| = 0 \Rightarrow \lambda^2 - \Gamma\lambda + \Delta = 0$$

$$\therefore \lambda = \lambda_1, \lambda_2 \text{ where, } \lambda_1 = \frac{\Gamma + \sqrt{\Gamma^2 - 4\Delta}}{2}, \lambda_2 = \frac{\Gamma - \sqrt{\Gamma^2 - 4\Delta}}{2}.$$

where  $\lambda_1$  and  $\lambda_2$  are eigenvalues of matrix C.

$$\text{Here, } \Gamma = \text{Tr}(J(x^*, y^*)) = C_{11} + C_{22} = -\frac{B\beta y^*}{(B-g+x^*)^2} + r_1 \left(1 - \frac{2x^*}{K}\right) - \frac{\eta_1 y^* x^{*2}}{A+x^{*2}}$$

$$\text{and } \Delta = \det(J(x^*, y^*)) = (C_{11}C_{22} - C_{12}C_{21})$$

$$= \frac{\beta y^* (x^* - g)}{(B-g+x^*)} \left( -\frac{2A\eta_1 x^* y^*}{(A+x^{*2})^2} + \frac{B\beta\gamma}{(B-g+x^*)^2} - \frac{r_2}{K} \right) + \frac{\eta_1 x^{*2} y^*}{(A+x^{*2})} \left( \frac{B\beta y^*}{(B-g+x^*)^2} + r_1 \left( \frac{2x^*}{K} - 1 \right) \right)$$

**Case I:** If  $\Gamma < 0$ ,  $\Delta > 0$ ,  $\Gamma^2 - 4\Delta \geq 0$ , then  $\lambda_1$  and  $\lambda_2$  are negative. So,  $E_I(x^*, y^*)$  is stable node.

**Case II:** If  $\Gamma > 0$ ,  $\Delta > 0$ ,  $\Gamma^2 - 4\Delta \geq 0$ , then  $\lambda_1$  and  $\lambda_2$  are positive. Therefore,  $E_I(x^*, y^*)$  is unstable node.

**Case III:** If  $\Gamma < 0$ ,  $\Gamma^2 - 4\Delta < 0$ , then  $\lambda_1$  and  $\lambda_2$  are imaginary whose real part is negative. Therefore,  $E_I(x^*, y^*)$  is stable spiral.

**Case IV:** If  $\Gamma > 0$ ,  $\Gamma^2 - 4\Delta < 0$ , then  $\lambda_1$  and  $\lambda_2$  are imaginary whose real part is positive. Hence,  $E_I(x^*, y^*)$  is unstable spiral.

**Case V:** If  $\Delta < 0$ , then between  $\lambda_1$  and  $\lambda_2$ , one is negative and another is positive (since  $\Delta = \lambda_1\lambda_2$ ). Hence,  $E_I(x^*, y^*)$  is unstable saddle.

**Case VI:** If  $\Gamma = 0$ ,  $\Delta > 0$ ,  $\lambda_1$  and  $\lambda_2$  are purely imaginary. So,  $E_I(x^*, y^*)$  is stable centre.

□

## 6. Bifurcation Analysis

In this particular section, our focus is directed towards an exhaustive exploration of all possible local bifurcations associated with system (2.1).

### 6.1. Transcritical Bifurcation

Transcritical bifurcation is the fundamental process by which an equilibrium point of the system changes its stability with another equilibrium point for a variation of a parameter. In this study, we demonstrate that system (2.1) undergoes a transcritical bifurcation with respect to the bifurcating parameter  $d_1$ . This results in a switch in stability between the interior equilibrium point and predator free equilibrium point  $E_a(K, 0)$ .

**Theorem 6.1.** *The system (2.1) experiences a transcritical bifurcation around the predator-free equilibrium point  $E_a(K, 0)$  at the bifurcation threshold  $d_1^{(TC)} = \frac{\beta\gamma(K-g)}{B-g+K}$ .*

*Proof.* In order to prove that system (2.1) undergoes a transcritical bifurcation around  $E_a(K, 0)$  at the bifurcation threshold  $d_1^{(TC)} = \frac{\beta\gamma(K-g)}{B-g+K}$ , we apply Sotomayor’s theorem [25]. Now the Jacobian matrix at  $E_a(K, 0)$  is

$$J(E_a)|_{d_1=d_1^{(TC)}} = \begin{bmatrix} -r_1 & -\frac{\beta(K-g)}{B-g+K} \\ 0 & 0 \end{bmatrix} = \tilde{M}$$

Now 0 is an eigen value of  $\tilde{M}$ . So, 0 is also an eigenvalue of  $\tilde{M}^T$  and let  $W$  and  $Z$  are eigenvectors corresponding to 0 of matrix  $\tilde{M}$  and  $\tilde{M}^T$  respectively. Here,  $W = \begin{pmatrix} 1 \\ w_1 \end{pmatrix}$ , and  $Z = \begin{pmatrix} 0 \\ 1 \end{pmatrix}$ , where,  $w_1 = -\frac{r_1(B-g+K)}{\beta(K-g)}$ .

Let  $H(x, y) = \begin{bmatrix} F(x, y) \\ G(x, y) \end{bmatrix}$ .

$\therefore H_{d_1} = \begin{bmatrix} 0 \\ -y \end{bmatrix}$ , so the transversality conditions for transcritical bifurcation are,

$Z^T [H_{d_1}(E_a; d_1 = d_1^{(TC)})] = 0,$

$Z^T [DH_{d_1}(E_a; d_1 = d_1^{(TC)}) W] = \frac{r_1(B-g+K)}{\beta(K-g)} \neq 0,$  (Since  $K > g$  and  $B > g$ )

$Z^T [D^2H(E_a; d_1 = d_1^{(TC)})(W, W)]$

$= -\frac{2r_1(B-g+K)}{\beta^2(K-g)^2} \left[ \frac{\eta_1 K^2 r_1 (B-g+K)}{A+K^2} + \frac{\beta^2 B \gamma (K-g)}{(B-g+K)^2} - \frac{r_2 \beta (K-g)}{K} \right] \neq 0$

provided,  $\frac{r_2 \beta (K-g)}{K} \neq \frac{\eta_1 K^2 r_1 (B-g+K)}{A+K^2} + \frac{\beta^2 B \gamma (K-g)}{(B-g+K)^2}$

So, by Sotomayor’s theorem, the system experiences a transcritical bifurcation around  $E_a(K, 0)$  at the bifurcation threshold  $d_1^{(TC)} = \frac{\beta\gamma(K-g)}{B-g+K}$ .

□

**Theorem 6.2.** *Around the predator-free equilibrium point  $E_a(K, 0)$ , system (2.1) experiences a transcritical bifurcation at the bifurcation threshold  $\beta^{(TC)} = \frac{\beta\gamma(K-g)}{B-g+K}$ .*

*Proof.* This proof can be obtained by following Theorem 6.1. □

### 6.2. Saddle-node Bifurcation

A saddle-node bifurcation arises when two equilibrium states within system (2.1) converge, collide, and disappear due to changes in a parametric value, resulting in their mutual annihilation and also it occurs,

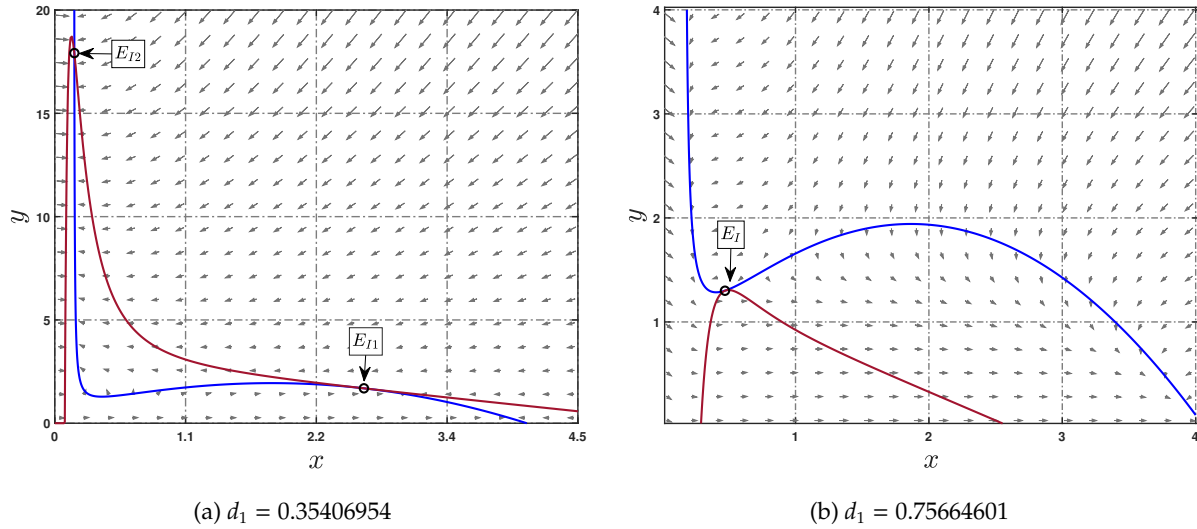


Figure 2: Non-trivial nullclines associated with saddle-node bifurcations. The blue curve represents the nontrivial prey nullcline, whereas the red curve represents the nontrivial predator nullcline.

when predator and prey nullclines meet tangentially. Figure 2 illustrates that the non-trivial prey and predator nullclines touch each other at two different values of  $d_1$ , with the other parameters values set to  $\{r_1 = 1.18, K = 4.06, \beta = 0.71, g = 0.164, B = 0.27, \gamma = 0.84, r_2 = 0.61, \eta_1 = 0.25, A = 0.5\}$ . Now we will provide a theorem that proves the occurrence of a saddle-node bifurcation in the system with respect to the bifurcation parameter  $d_1$ .

**Theorem 6.3.** System (2.1) exhibits a saddle-node bifurcation corresponding to the bifurcation parameter  $d_1$  at  $d_1 = d_1^{(SN_1)}$  and  $d_1 = d_1^{(SN_2)}$ .

*Proof.* Suppose  $x_{I1}$  be the repeated positive root of  $\phi(x) = 0$ , with  $\phi(x) \equiv a_6x^6 + a_5x^5 + a_4x^4 + a_3x^3 + a_2x^2 + a_1x + a_0$ . In section 4.2, we have provided the coefficients  $a_0, a_1, a_2, a_3, a_4, a_5$  and  $a_6$ . If the nontrivial nullcline

$$F(x, y) = 0 \text{ intersects the nontrivial nullcline } f_2(x, y) = 0 \text{ tangentially at } E_{I1}, \text{ then } \left. \frac{dy^{(F)}}{dx} \right|_{E_{I1}} = \left. \frac{dy^{(f_2)}}{dx} \right|_{E_{I1}}.$$

Jacobian matrix  $J(x, y)$  at  $d_1 = d_1^{(SN_1)}$  is as follows:

$$J(x, y) = \begin{bmatrix} \frac{\partial F}{\partial x} & \frac{\partial F}{\partial y} \\ y \frac{\partial f_2}{\partial x} & y \frac{\partial f_2}{\partial y} \end{bmatrix}_{E_{I1}, d_1^{(SN_1)}} \quad \left( \because f_2|_{E_{I1}} = 0 \right)$$

$$= \begin{bmatrix} \frac{r_1(K - 2x)}{K} - \frac{\beta y B}{(B + x - g)^2} & -\frac{\beta(x - g)}{B + x - g} \\ \frac{\gamma \beta B y}{(B + x - g)^2} - \frac{r_2 y}{K} - \frac{2\eta_1 x y^2 A}{(A + x^2)^2} & -\frac{\eta_1 x^2 y}{A + x^2} \end{bmatrix}_{E_{I1}, d_1^{(SN_1)}}$$

Now,

$$\det(J(x, y)) = \left[ y \left( \frac{\partial F}{\partial x} \frac{\partial f_2}{\partial y} - \frac{\partial f_2}{\partial x} \frac{\partial F}{\partial y} \right) \right]_{E_{I1}, d_1^{(SN_1)}} = \left[ y \frac{\partial F}{\partial y} \frac{\partial f_2}{\partial y} \left( \frac{dy^{(f_2)}}{dx} - \frac{dy^{(F)}}{dx} \right) \right]_{E_{I1}, d_1^{(SN_1)}} = 0.$$

Let  $J(x, y) = P$  and  $J^T(x, y) = Q$ . As  $\det(J(x, y)) = 0$ , so 0 is an eigenvalue of both  $P$  and  $Q$ . The eigenvectors corresponding to  $P$  and  $Q$  are given by  $W = \begin{bmatrix} w_1 \\ w_2 \end{bmatrix}_{E_{11}, d_1^{(SN_1)}}$  and  $Z = \begin{bmatrix} z_1 \\ z_2 \end{bmatrix}_{E_{11}, d_1^{(SN_1)}}$  respectively, where  $w_1 = 1$ ,

$$w_2 = -\frac{r_1(K - 2x)(B - g + x)^2 - B\beta Ky}{\beta K(B + x - g)(g - x)}, z_1 = 1 \text{ and } z_2 = -\frac{\beta(A + x^2)(x - g)}{\eta_1 x^2 y(B - g + x)}.$$

Applying the Sotomayor’s theorem [25] at  $d_1 = d_1^{(SN_1)}$ , we get

$$Z^T \tilde{F}_{d_1}(E_{11}, d_1^{(SN_1)}) = -y' \neq 0$$

$$Z^T [D^2 \tilde{F}(E_{11}, d_1^{(SN_1)})(W, W)] = \mathcal{R} - \frac{2r_1}{K} \neq 0, \quad \text{provided, } \mathcal{R} \neq \frac{2r_1}{K}$$

where,  $\mathcal{R} = \mathcal{L} + \mathcal{M} + \mathcal{N}$  and

$$\mathcal{L} = \left[ \frac{2(\beta^2 BK^2 y^2 (2B - g + x) + 3\beta BK r_1 y (2x - K)(B - g + x)^2 + r_1^2 (K - 2x)^2 (B - g + x)^4)}{\beta K^2 y (x - g)(B - g + x)^3} \right]_{E_{11}, d_1^{(SN_1)}}$$

$$\mathcal{M} = \left[ \frac{2(A + x^2)(r_1(2x - K)(B - g + x)^2 + \beta BK y)}{\eta_1 K x^2 y (B - g + x)^2} \left( \frac{4A\eta_1 x y}{(A + x^2)^2} - \frac{B\gamma\beta}{(B - g + x)^2} + \frac{r_2}{K} \right) \right]_{E_{11}, d_1^{(SN_1)}}$$

$$\mathcal{N} = \left[ \frac{\beta(A + x^2)(g - x)}{\eta_1 x^2 (B - g + x)} \left( \frac{2A\eta_1 y(A - 3x^2)}{(A + x^2)^3} + \frac{2B\gamma\beta}{(B - g + x)^3} \right) \right]_{E_{11}, d_1^{(SN_1)}}$$

Here,  $\tilde{F} = \begin{pmatrix} F \\ G \end{pmatrix}$ , each of  $F$  and  $G$  is specified in equation (2.1). Therefore, the system satisfies the required conditions needed for a saddle-node bifurcation around the interior equilibrium  $E_{11}$  at  $d_1 = d_1^{(SN_1)}$ . In a similar way, there is another saddle-node bifurcation occurring at a different interior equilibrium point at  $d_1 = d_1^{(SN_2)}$ .

□

**Theorem 6.4.** The system (2.1) exhibits saddle-node bifurcation at  $\beta = \beta^{(SN_1)}$  and  $\beta = \beta^{(SN_2)}$  with respect to  $\beta$ .

*Proof.* Let us skip this proof as it is similar to previous one (Theorem 6.3). □

**Theorem 6.5.** For parameter  $\eta_1$ , system (2.1) experiences saddle-node bifurcation at  $\eta_1 = \eta_1^{(SN_1)}$  and  $\eta_1 = \eta_1^{(SN_2)}$ .

*Proof.* Let us omit this proof as it is similar to Theorem 6.3. □

**Theorem 6.6.** System (2.1) exhibits saddle-node bifurcation at  $r_2 = r_2^{(SN_1)}$  and  $r_2 = r_2^{(SN_2)}$  for bifurcation parameter  $r_2$ .

*Proof.* This proof can be obtained by following Theorem 6.3. □

### 6.3. Hopf-bifurcation

Using  $r_2$  as a variable parameter, the characteristic equation of (2.1) for  $J(x, y)$  can be represented as follows:

$$\lambda^2 - \Gamma(r_2)\lambda + \Delta(r_2) = 0 \tag{6.1}$$

where  $\Gamma(r_2)$ ,  $\Delta(r_2)$  are trace and determinant of  $J(x, y)$  at  $E_I(x^*, y^*)$  respectively (mentioned in Theorem 5.3). Suppose the purely imaginary roots of (6.1) appear at the point  $r_2 = r_2^{(H)}$ . Then  $\Gamma(r_2^{(H)}) = 0$ , and  $\Delta(r_2^{(H)}) > 0$ . Let us prove the existence of Hopf-bifurcation in (2.1) at  $r_2 = r_2^{(H)}$ .

**Theorem 6.7.** System (2.1) experiences a Hopf-bifurcation around  $E_1(x^*, y^*)$  at  $r_2 = r_2^{(H)}$ , when  $\Gamma(r_2^{(H)}) = 0, \Delta(r_2^{(H)}) > 0$  and  $\left[\frac{d\Gamma}{dr_2}\right]_{r_2=r_2^{(H)}} \neq 0$ .

*Proof.* At  $r_2 = r_2^{(H)}, \Gamma(r_2^{(H)}) = 0, \Delta(r_2^{(H)}) > 0$ , the characteristic equation has purely imaginary roots, i.e.  $\lambda_1 = i\sqrt{\Delta(r_2^{(H)})}$  and  $\lambda_2 = -i\sqrt{\Delta(r_2^{(H)})}$ . Hence,  $\lambda_1 = g_1(r_2) + ig_2(r_2)$  and  $\lambda_2 = g_1(r_2) - ig_2(r_2)$  are the roots of (6.1) in an open neighbourhood of  $r_2^{(H)}$ , where  $g_1(r_2), g_2(r_2) \in \mathbb{R}$ . By utilizing the Hopf-Bifurcation Theorem [23], it can be inferred that the stability of (2.1) transits through a Hopf-bifurcation, provided the following transversality condition

$$\left[\frac{d}{dr_2}(Re(\lambda_i(r_2)))\right]_{r_2=r_2^{(H)}} = \left[\frac{dg_1(r_2)}{dr_2}\right]_{r_2=r_2^{(H)}} \neq 0$$

is satisfied. Let us put  $\lambda(r_2) = g_1(r_2) + ig_2(r_2)$  in equation (6.1), then we get,

$$(g_1(r_2) + ig_2(r_2))^2 - \Gamma(r_2)(g_1(r_2) + ig_2(r_2)) + \Delta(r_2) = 0$$

If we differentiate both sides w.r.t.  $r_2$  we get,

$$2(g_1(r_2) + ig_2(r_2))(g_1(r_2) + ig_2(r_2)) - \Gamma(r_2)(g_1(r_2) + ig_2(r_2)) - \dot{\Gamma}(r_2)(g_1(r_2) + ig_2(r_2)) + \dot{\Delta}(r_2) = 0$$

Comparing and solving the real and imaginary parts of both sides yields:

$$g_1 = -\frac{(X_1X_3 + X_2X_4)}{X_1^2 + X_2^2} \tag{6.2}$$

where,  $X_1 = (2g_1 - \Gamma), X_2 = 2g_2, X_3 = (\dot{\Delta} - \dot{\Gamma}g_1), X_4 = -\dot{\Gamma}g_2$ .

At  $r_2 = r_2^{(H)}; g_1 = 0, g_2 = \pm\sqrt{\Delta}$  which gives,  $X_1 = 0, X_2 = \pm 2\sqrt{\Delta}, X_3 = \dot{\Delta}$  and  $X_4 = \mp\dot{\Gamma}\sqrt{\Delta}$ . Then:

$$[g_1]_{r_2=r_2^{(H)}} = \left[\frac{dg_1(r_2)}{dr_2}\right]_{r_2=r_2^{(H)}} = \pm\frac{1}{2}\left[\frac{d\Gamma(r_2)}{dr_2}\right]_{r_2=r_2^{(H)}} \neq 0$$

This completes the proof.  $\square$

**Theorem 6.8.** For parameter  $d_1$ , a Hopf-bifurcation occurs in system (2.1) around  $E_1(x^*, y^*)$  at  $d_1 = d_1^{(H)}$ , provided  $\Gamma(d_1^{(H)}) = 0, \Delta(d_1^{(H)}) > 0$  and  $\left[\frac{d\Gamma}{dd_1}\right]_{d_1=d_1^{(H)}} \neq 0$ .

*Proof.* Let us skip this as it can be obtained by following Theorem 6.7.  $\square$

#### 6.4. Bogdanov-Takens bifurcation

It is evident that system (2.1) experiences both saddle-node bifurcation and Hopf-bifurcation for a suitable collection of parametric values. Within a specific two-parametric bifurcation plane, these two bifurcation points can result in the formation of a saddle-node bifurcation curve and a Hopf-bifurcation curve. When the Hopf-bifurcation curve intersects with the saddle-node bifurcation curve, a new bifurcation called Bogdanov-Takens bifurcation arises. Usually, a Bogdanov-Takens (BT) bifurcation refers to a point, in which the Jacobian matrix has a zero eigenvalue with algebraic multiplicity two. We will now provide a theorem demonstrating that, system (2.1) goes Bogdanov-Takens bifurcation for the bifurcation parameters  $\beta$  and  $r_2$ .

**Theorem 6.9.** System (2.1) undergoes a Bogdanov-Takens bifurcation around the interior equilibrium point  $E_1(x^*, y^*)$  with respect to the bifurcation parameters  $\beta, r_2$ , whenever  $E_1(x^*, y^*)$  satisfies the following conditions:

(BT1)  $tr(J(E_1; (\beta^{BT}, r_2^{BT}))) = 0$

(BT2)  $det(J(E_1; (\beta^{BT}, r_2^{BT}))) = 0$

*Proof.* Conditions (BT1) and (BT2) are equivalent to following:

$$-\frac{B\beta y^*}{(B-g+x^*)^2} + r_1 \left(1 - \frac{2x^*}{K}\right) - \frac{\eta_1 y^* x^{*2}}{A+x^{*2}} = 0$$

$$\frac{\beta y^*(x^*-g)}{(B-g+x^*)} \left( -\frac{2A\eta_1 x^* y^*}{(A+x^{*2})^2} + \frac{B\beta\gamma}{(B-g+x^*)^2} - \frac{r_2}{K} \right) + \frac{\eta_1 x^{*2} y^*}{(A+x^{*2})} \left( \frac{B\beta y^*}{(B-g+x^*)^2} + r_1 \left( \frac{2x^*}{K} - 1 \right) \right) = 0$$

From above equations we can write explicitly

$$\beta^{BT} = \frac{(B-g+x^*)^2 (AKr_1 - 2Ar_1x^* + Kr_1x^{*2} - \eta_1 Kx^{*2}y^* - 2r_1x^{*3})}{BK y^* (A+x^{*2})},$$

$$r_2^{BT} = \frac{\gamma (r_1 (A+x^{*2}) (2x^*-K) + \eta_1 Kx^{*2}y^*)}{y^* (A+x^{*2})} + \frac{2A\eta_1 Kx^*y^*}{(A+x^{*2})^2}$$

$$+ \frac{B\eta_1^2 K^2 x^{*4} y^{*2}}{(A+x^{*2})(x^*-g)(B-g+x^*)(r_1(A+x^{*2})(K-2x^*) - \eta_1 Kx^{*2}y^*)}$$

Let us consider a small perturbation around the bifurcation threshold  $(\beta^{BT}, r_2^{BT})$ , say  $(\beta^{BT} + \lambda_1, r_2^{BT} + \lambda_2)$ , where  $\{\lambda_i; i = 1, 2\}$  are sufficiently small.

Then system (2.1) becomes

$$\frac{dx}{dt} = r_1 x \left(1 - \frac{x}{K}\right) - \frac{(\beta^{BT} + \lambda_1)(x-g)y}{B+x-g} \equiv G_1(x, y, \lambda_1) = F(x, y) - \frac{\lambda_1(x-g)y}{B+x-g}$$

$$\frac{dy}{dt} = \frac{\gamma(\beta^{BT} + \lambda_1)(x-g)y}{B+x-g} + (r_2^{BT} + \lambda_2)y \left(1 - \frac{x}{K}\right) - d_1 y - \frac{\eta_1 x^2 y^2}{A+x^2}$$

$$\equiv G_2(x, y, \lambda_2) = G(x, y) + \lambda_2 y \left(1 - \frac{x}{K}\right) + \frac{\lambda_1 \gamma (x-g)y}{B+x-g}$$
(6.3)

Now we shift the equilibrium point  $E_I(x^*, y^*)$  to the origin by the transformations  $x_1 = x - x^*$  and  $x_2 = y - y^*$ . So system (6.3) becomes

$$\frac{dx_1}{dt} = p_{00} + p_{10}x_1 + p_{01}x_2 + \frac{p_{11}}{2}x_1^2 + p_{12}x_1x_2 + \frac{p_{22}}{2}x_2^2 + \dots$$

$$\frac{dx_2}{dt} = q_{00} + q_{10}x_1 + q_{01}x_2 + \frac{q_{11}}{2}x_1^2 + q_{12}x_1x_2 + \frac{q_{22}}{2}x_2^2 + \dots$$
(6.4)

where,

$$p_{00} = G_1(x^*, y^*, \lambda_1, \lambda_2), \quad q_{00} = G_2(x^*, y^*, \lambda_1, \lambda_2), \quad p_{10} = \frac{\partial G_1}{\partial x}(x^*, y^*, \lambda_1, \lambda_2) = a - \frac{B\lambda_1 y^*}{(B-g+x^*)^2}$$

$$q_{10} = \frac{\partial G_2}{\partial x}(x^*, y^*, \lambda_1, \lambda_2) = b - \frac{\lambda_2 y^*}{K} + \frac{B\gamma\lambda_1 y^*}{(B-g+x^*)^2}, \quad p_{01} = \frac{\partial G_1}{\partial y}(x^*, y^*, \lambda_1, \lambda_2) = c - \frac{\lambda_1(x^*-g)}{B-g+x^*}$$

$$q_{01} = \frac{\partial G_2}{\partial y}(x^*, y^*, \lambda_1, \lambda_2) = d + \lambda_2 \left(1 - \frac{x^*}{K}\right) + \frac{\lambda_1 \gamma (x^*-g)}{B+x^*-g}, \quad p_{22} = \frac{\partial^2 G_1}{\partial y^2}(x^*, y^*, \lambda_1, \lambda_2) = 0$$

$$p_{11} = \frac{\partial^2 G_1}{\partial x^2}(x^*, y^*, \lambda_1, \lambda_2) = \frac{2By^*(\beta^{BT} + \lambda_1)}{(B-g+x^*)^3} - \frac{2r_1}{K}, \quad q_{22} = \frac{\partial^2 G_2}{\partial y^2}(x^*, y^*, \lambda_1, \lambda_2) = -\frac{2\eta_1 x^{*2}}{A+x^{*2}}$$

$$q_{11} = \frac{\partial^2 G_2}{\partial x^2}(x^*, y^*, \lambda_1, \lambda_2) = -\frac{2A\eta_1 y^{*2}(A-3x^{*2})}{(A+x^{*2})^3} - \frac{2B\gamma y^*(\beta + \lambda_1)}{(B-g+x^*)^3}$$

$$p_{12} = \frac{\partial^2 G_1}{\partial y \partial x}(x^*, y^*, \lambda_1, \lambda_2) = -\frac{B(\beta^{BT} + \lambda_1)}{(B-g+x^*)^2}$$

$$q_{12} = \frac{\partial^2 G_2}{\partial y \partial x}(x^*, y^*, \lambda_1, \lambda_2) = -\frac{4A\eta_1 x^* y^*}{(A + x^{*2})^2} + \frac{B\gamma(\beta + \lambda_1)}{(B - g + x^*)^2} - \frac{\lambda_2 + r_2}{K}$$

Here,  $a = -\frac{B\beta y^*}{(B - g + x^*)^2} + r_1 \left(1 - \frac{2x^*}{K}\right)$ ,  $b = -\frac{\beta(x^* - g)}{B - g + x^*}$ ,  $c = -\frac{2A\eta_1 x^* y^{*2}}{(A + x^{*2})^2} + \frac{B\gamma\beta\gamma}{(B - g + x^*)^2} - \frac{r_2 y^*}{K}$ ,  
 $d = -\frac{\eta_1 y^* x^{*2}}{A + x^{*2}}$ .

Now, introducing affine transformation [25]  $z_1 = x_1, z_2 = ax_1 + bx_2$ , then the above system is transformed into

$$\begin{aligned} \frac{dz_1}{dt} &= z_2 + \zeta_{00}(\lambda) + \zeta_{10}(\lambda)z_1 + \zeta_{01}(\lambda)z_2 + \frac{\zeta_{20}(\lambda)}{2}z_1^2 + \zeta_{11}z_1z_2 + \frac{\zeta_{02}(\lambda)}{2}z_2^2 + B_1(z_1, z_2) \\ \frac{dz_2}{dt} &= \eta_{00}(\lambda) + \eta_{10}(\lambda)z_1 + \eta_{01}(\lambda)z_2 + \frac{\eta_{20}(\lambda)}{2}z_1^2 + \eta_{11}z_1z_2 + \frac{\eta_{02}}{2}z_2^2 + B_2(z_1, z_2) \end{aligned} \tag{6.5}$$

where,  $\lambda = (\lambda_1, \lambda_2)$  and  $B_1(z_1, z_2), B_2(z_1, z_2)$  are  $C^\infty$  functions at least of third order with respect to  $(z_1, z_2)$ .

$$\begin{aligned} \zeta_{00}(\lambda) &= G_1(x^*, y^*, \lambda), \quad \eta_{00}(\lambda) = aG_1(x^*, y^*, \lambda) + bG_2(x^*, y^*, \lambda), \quad \zeta_{10}(\lambda) = \left(p_{10} - \frac{a}{b}p_{01}\right), \\ \eta_{10}(\lambda) &= bq_{10} - aq_{01} + ap_{10} - \frac{a^2}{b}p_{01}, \quad \zeta_{01}(\lambda) = \frac{1}{b}p_{01} - 1, \quad \eta_{01}(\lambda) = q_{01} + \frac{a}{b}p_{01}, \quad \zeta_{02}(\lambda) = \frac{p_{22}}{b^2}, \\ \zeta_{20}(\lambda) &= \left[p_{11} - \frac{2ap_{12}}{b} + \frac{a^2p_{22}}{b^2}\right], \quad \eta_{20}(\lambda) = \left[ap_{11} + bq_{11} - \frac{2a(ap_{12} + bq_{12})}{b} + \frac{a^2(ap_{22} + bq_{22})}{b^2}\right], \\ \zeta_{11}(\lambda) &= \left[\frac{p_{12}}{b} - \frac{ap_{22}}{b^2}\right], \quad \eta_{11}(\lambda) = \left[\frac{(ap_{12} + bq_{12})}{b} - \frac{a(ap_{22} + bq_{22})}{b^2}\right], \quad \eta_{02}(\lambda) = \frac{(ap_{22} + bq_{22})}{b^2}. \end{aligned}$$

The degeneracy conditions of the Bogdanov-Takens bifurcations at  $(\beta^{BT}, r_2^{BT})$  are,

$$\text{I. } \begin{bmatrix} a & b \\ c & d \end{bmatrix} \neq \begin{bmatrix} 0 & 0 \\ 0 & 0 \end{bmatrix}$$

$$\text{II. } \zeta_{20}(0) + \eta_{11}(0) = R_1 \neq 0$$

$$\begin{aligned} \text{where, } R_1 &= \frac{2\gamma r_1(K-2x^*)}{Ky^*} - \frac{2\gamma\eta_1 x^{*2}}{A+x^{*2}} + \frac{2\eta_1 x^* y^* (Ax^*(2B-7g)+3Ag(g-B)+4Ax^{*2}-x^{*3}(B+g)+x^{*4})}{(A+x^{*2})^2(g-x^*)(B-g+x^*)} \\ &+ \frac{3Br_1^2(A+x^{*2})(K-2x^*)^2}{K(g-x^*)(B-g+x^*)(r_1(A+x^{*2})(K-2x^*)-\eta_1 Kx^{*2}y^*)} + \frac{r_1(2x^*(4B-4g-K+3x^*)-B(2g+3K)+2g(g+K))}{K(g-x^*)(B-g+x^*)} \end{aligned}$$

Also,

$$\text{III. } \eta_{20} = \frac{2R_2}{(A + x^{*2})^4}$$

$$\begin{aligned} \text{where, } R_2 &= -\frac{B\eta_1^3 Kx^{*6}y^{*3}(A+x^{*2})^2}{(g-x^*)(B-g+x^*)(r_1(A+x^{*2})(K-2x^*)-\eta_1 Kx^{*2}y^*)} - \frac{\eta_1 x^{*2} y^* (A+x^{*2})^2 (r_1(A+x^{*2})(B-g-K+3x^*)+\eta_1 Kx^{*2}y^*)}{K(B-g+x^*)} \\ &+ \frac{B\eta_1^3 Kx^{*6}y^{*3}(A+x^{*2})^2}{(x^*-g)(B-g+x^*)(r_1(A+x^{*2})(K-2x^*)-\eta_1 Kx^{*2}y^*)} + \frac{B\eta_1^2 x^{*4} y^{*2} (A+x^{*2})^2}{(g-x^*)(B-g+x^*)} + \frac{2\gamma\eta_1 x^{*2} (A+x^{*2})^2 (\eta_1 Kx^{*2}y^* - r_1(A+x^{*2})(K-2x^*))}{K} \\ &+ \frac{(g-x^*)(r_1(A+x^{*2})(K-2x^*)-\eta_1 Kx^{*2}y^*)(\eta_1 Ky^*(\gamma x^{*2}(A+x^{*2})^2 - Ay^*(A-3x^{*2})(B-g+x^*)) - \gamma r_1(A+x^{*2})^3(K-2x^*))}{BK^2 y^*} \\ &+ 6A\eta_1^2 x^{*3} y^{*2} (A + x^{*2}) \end{aligned}$$

Therefore,  $\zeta_{20}(0) + \eta_{11}(0) \neq 0$  and  $\eta_{20}(0)$  may or may not be 0. So, when  $\eta_{20}(0) \neq 0$ , then according to **sign** [ $\eta_{20}(0) (\zeta_{20}(0) + \eta_{11}(0))$ ], i.e., either +1 or -1, the predator-prey model undergoes a subcritical BT bifurcation or undergoes a supercritical BT bifurcation respectively. It is difficult to show that  $\eta_{20}(0) \neq 0$  but we can assure the existence of Bogdanov-Takens bifurcation numerically for certain choice of parameters

shown in Section 7.2.  $\square$

**Theorem 6.10.** System (2.1) experiences a Bogdanov–Takens bifurcation around the interior equilibrium point  $E_I(x^*, y^*)$  with respect to the bifurcation parameters  $\eta_1, r_2$ , whenever  $E_I(x^*, y^*)$  satisfies the following conditions:

$$(BT1) \operatorname{tr}(J(E_I; (\eta_1^{BT}, r_2^{BT}))) = 0$$

$$(BT2) \det(J(E_I; (\eta_1^{BT}, r_2^{BT}))) = 0$$

*Proof.* We have omitted this proof as it is similar to Theorem 6.9.  $\square$

**Theorem 6.11.** System (2.1) exhibits a Bogdanov–Takens bifurcation around the interior equilibrium point  $E_I(x^*, y^*)$  with respect to the bifurcation parameters  $d_1, \beta$ , whenever  $E_I(x^*, y^*)$  satisfies the following conditions:

$$(BT1) \operatorname{tr}(J(E_I; (d_1^{BT}, \beta^{BT}))) = 0$$

$$(BT2) \det(J(E_I; (d_1^{BT}, \beta^{BT}))) = 0$$

*Proof.* Proceeding as in Theorem 6.9, the results can be obtained.  $\square$

### 6.5. Generalized Hopf-bifurcation

A stable limit cycle is formed by a supercritical Hopf-bifurcation when the first Lyapunov coefficient is negative ( $\sigma < 0$ ). Conversely, an unstable limit cycle is formed through a subcritical Hopf-bifurcation when the first Lyapunov coefficient is positive ( $\sigma > 0$ ). Therefore, when  $\sigma = 0$ , system (2.1) undergoes a generalized Hopf-bifurcation in two-parametric bifurcation plane. This point of bifurcation signifies the shift from subcritical to supercritical Hopf-bifurcation. We provide a theorem that establishes the existence of a generalized Hopf-bifurcation in system (2.1), specifically in relation to the bifurcation parameters  $\beta$  and  $d_1$ .

**Theorem 6.12.** System (2.1) undergoes a Bautin (Generalized Hopf) bifurcation at the interior equilibrium point  $E_I(x^*, y^*)$  when it reaches the bifurcation threshold  $(\beta^{GH}, d_1^{GH})$ , whenever the value of  $E_I(x^*, y^*)$  meets the following requirements:

$$(GH1) T = \operatorname{tr}(J(E_I; (\beta^{GH}, d_1^{GH}))) = 0$$

$$(GH2) D = \det(J(E_I; (\beta^{GH}, d_1^{GH}))) > 0$$

$$(GH3) L(E_I; (\beta^{GH}, d_1^{GH})) = 0$$

where  $L$  is the first Lyapunov number.

*Proof.* Let the nontrivial equilibrium point  $E_I(x^*, y^*)$  satisfies the above three conditions. The Jacobian matrix at  $E_I$  is

$$J(E_I) = \begin{bmatrix} \frac{\partial F}{\partial x} & \frac{\partial F}{\partial y} \\ y \frac{\partial f_2}{\partial x} & y \frac{\partial f_2}{\partial y} \end{bmatrix}_{E_I} \left( \because f_2|_{E_I} = 0 \right)$$

$$= \begin{bmatrix} \frac{r_1(K - 2x^*)}{K} - \frac{\beta y^* B}{(B + x^* - g)^2} & -\frac{\beta(x^* - g)}{B + x^* - g} \\ \frac{\gamma \beta B y^*}{(B + x^* - g)^2} - \frac{r_2 y^*}{K} - \frac{2\eta_1 x^* y^{*2} A}{(A + x^{*2})^2} & -\frac{\eta_1 x^{*2} y^*}{A + x^{*2}} \end{bmatrix}$$

Now, from the conditions (GH1) and (GH2):

$$\beta_{GH} = \frac{(B - g + x^*)^2 (AKr_1 - 2Ar_1x^* + Kr_1x^{*2} - \eta_1Kx^{*2}y^* - 2r_1x^{*3})}{BK y^* (A + x^{*2})}$$

To find the first Lyapunov number  $L$  at  $E_I$ , we shift  $E_I$  to origin by using the transformation  $x_1 = x - x^*$  and  $x_2 = y - y^*$ . So, system (2.1) becomes

$$\begin{aligned} \frac{dx_1}{dt} &= ax_1 + bx_2 + P(x_1, x_2) \\ \frac{dx_2}{dt} &= cx_1 + dx_2 + Q(x_1, x_2) \end{aligned}$$

where,  $a = \left(\frac{\partial F}{\partial x}\right)_{E_I}$ ,  $b = \left(\frac{\partial F}{\partial y}\right)_{E_I}$ ,  $c = \left(\frac{\partial G}{\partial x}\right)_{E_I}$ ,  $d = \left(\frac{\partial G}{\partial y}\right)_{E_I}$  and  $P(x_1, x_2)$ ,  $Q(x_1, x_2)$  are analytic functions, defined by

$$\begin{aligned} P(x_1, x_2) &= \sum_{i+j \geq 2} a_{ij} x_1^i x_2^j \\ Q(x_1, x_2) &= \sum_{i+j \geq 2} b_{ij} x_1^i x_2^j \end{aligned}$$

where,  $a_{ij}$  and  $b_{ij}$  are defined by,  $a_{ij} = \frac{1}{i! j!} \left(\frac{\partial^{i+j} F}{\partial x^i \partial y^j}\right)_{E_I}$  and  $b_{ij} = \frac{1}{i! j!} \left(\frac{\partial^{i+j} G}{\partial x^i \partial y^j}\right)_{E_I}$ .

Now, the first Lyapunov number is as follows;

$$L = -\frac{3\pi}{2bD^{\frac{3}{2}}} \left[ \left\{ ac(a_{11}^2 + a_{11}b_{02} + a_{02}b_{11}) + ab(b_{11}^2 + a_{20}b_{11} + a_{11}b_{02}) + c^2(a_{11}a_{02} + 2a_{02}b_{02}) - 2ac(b_{02}^2 - a_{20}a_{02}) - 2ab(a_{20}^2 - b_{20}b_{02}) - b^2(2a_{20}b_{20} + b_{11}b_{20}) + (bc - 2a^2)(b_{11}b_{02} - a_{11}a_{20}) \right\} - (a^2 + bc) \left\{ 3(cb_{03} - ba_{30}) + 2a(a_{21} + b_{12}) + (ca_{12} - bb_{21}) \right\} \right]$$

Let us determine the coefficients  $a_{ij}$ ,  $b_{ij}$  and  $a, b, c$  and  $d$  to calculate the first Lyapunov number.

$$\begin{aligned} a &= \frac{\partial F}{\partial x}(x^*, y^*) = \frac{r_1(K - 2x^*)}{K} - \frac{\beta y^* B}{(B + x^* - g)^2}, \quad b = \frac{\partial F}{\partial y}(x^*, y^*) = -\frac{\beta(x^* - g)}{B + x^* - g}, \\ c &= \frac{\partial G}{\partial x}(x^*, y^*) = \frac{\gamma \beta B y^*}{(B + x^* - g)^2} - \frac{r_2 y^*}{K} - \frac{2\eta_1 x^* y^{*2} A}{(A + x^{*2})^2}, \quad d = \frac{\partial G}{\partial y}(x^*, y^*) = -\frac{\eta_1 x^{*2} y^*}{A + x^{*2}}, \\ a_{11} &= \frac{\partial^2 F}{\partial y \partial x}(x^*, y^*) = -\frac{\beta B}{(B - g + x^*)^2}, \quad a_{20} = \frac{1}{2} \frac{\partial^2 F}{\partial x^2}(x^*, y^*) = \frac{\beta B y^*}{(B - g + x^*)^3} - \frac{r_1}{K}, \\ a_{02} &= \frac{1}{2} \frac{\partial^2 F}{\partial y^2}(x^*, y^*) = 0, \quad a_{21} = \frac{1}{2} \frac{\partial^3 F}{\partial x^2 \partial y}(x^*, y^*) = \frac{\beta B}{(B - g + x^*)^3}, \quad a_{12} = \frac{1}{2} \frac{\partial^3 F}{\partial x \partial y^2}(x^*, y^*) = 0, \\ a_{30} &= \frac{1}{6} \frac{\partial^3 F}{\partial x^3}(x^*, y^*) = -\frac{\beta B y^*}{(B - g + x^*)^4}, \quad a_{03} = \frac{1}{6} \frac{\partial^3 F}{\partial y^3}(x^*, y^*) = 0, \quad b_{03} = \frac{1}{6} \frac{\partial^3 G}{\partial y^3}(x^*, y^*) = 0, \\ b_{11} &= \frac{\partial^2 G}{\partial y \partial x}(x^*, y^*) = -\frac{4A\eta_1 x^* y^*}{(A + x^{*2})^2} + \frac{B\gamma\beta}{(B - g + x^*)^2} - \frac{r_2}{K}, \quad b_{12} = \frac{1}{2} \frac{\partial^3 G}{\partial x \partial y^2}(x^*, y^*) = -\frac{2A\eta_1 x^*}{(A + x^{*2})^2}, \\ b_{20} &= \frac{1}{2} \frac{\partial^2 G}{\partial x^2}(x^*, y^*) = -\frac{A\eta_1 y^{*2} (A - 3x^{*2})}{(A + x^{*2})^3} - \frac{B\gamma\beta y^*}{(B - g + x^*)^3}, \quad b_{02} = \frac{1}{2} \frac{\partial^2 G}{\partial y^2}(x^*, y^*) = -\frac{\eta_1 x^{*2}}{A + x^{*2}}, \\ b_{21} &= \frac{1}{2} \frac{\partial^3 G}{\partial x^2 \partial y}(x^*, y^*) = -\frac{2A\eta_1 y^* (A - 3x^{*2})}{(A + x^{*2})^3} - \frac{B\gamma\beta}{(B - g + x^*)^3}, \\ b_{30} &= \frac{1}{6} \frac{\partial^3 G}{\partial x^3}(x^*, y^*) = \frac{4A\eta_1 x^* y^{*2} (A - x^{*2})}{(A + x^{*2})^4} + \frac{B\gamma\beta y^*}{(B - g + x^*)^4}. \end{aligned}$$

Substituting the values of above expressions in first Lyapunov number and after some algebraic computations, we obtain,

$$L = -\frac{3\pi \cdot (\mathcal{Q}_1 + \mathcal{Q}_2 + \mathcal{Q}_3 + \mathcal{Q}_4 + \mathcal{Q}_5 + \mathcal{Q}_6 + \mathcal{Q}_7)}{2bD^{\frac{3}{2}}} \text{ where,}$$

$$\mathcal{Q}_1 = -2B^2\eta_1^3K^3(x^*)^6(y^*)^3(A + (x^*)^2)(B - g + x^*) \cdot [-2A\eta_1Kx^*y^*(B - g + x^*)^2 - r_2(A + (x^*)^2)^2(B - g + x^*)^2 + B\gamma\beta K(A + (x^*)^2)^2]$$

$$\mathcal{Q}_2 = B^2\eta_1Kr_1(x^*)^2y^*(A + (x^*)^2)^3(K - 2x^*)(B - g + x^*)[r_1(A + (x^*)^2)(K - 2x^*) - \eta_1K(x^*)^2y^*] \cdot [-2A\eta_1Kx^*y^*(B - g + x^*)^2 - r_2(A + (x^*)^2)^2(B - g + x^*)^2 + B\gamma\beta K(A + (x^*)^2)^2]$$

$$\mathcal{Q}_3 = K(g - x^*)^2(r_1(A + (x^*)^2)(K - 2x^*) - \eta_1K(x^*)^2y^*)^2 \cdot [A\eta_1y^*(A - 3(x^*)^2)(B - g + x^*)^3 + B\gamma\beta(A + (x^*)^2)^3] \cdot [-2r_1(A + (x^*)^2)^2(B - g + x^*)(B - g - K + 3x^*) - 2\eta_1Kx^*y^*(B - g + x^*) \cdot (2AB - 2Ag + 3Ax^* + (x^*)^3) - r_2(A + (x^*)^2)^2(B - g + x^*)^2 + B\gamma\beta K(A + (x^*)^2)^2]$$

$$\mathcal{Q}_4 = B(A + (x^*)^2)[(A + (x^*)^2)(B - g + x^*)(r_1(A + (x^*)^2)(K - 2x^*) - \eta_1K(x^*)^2y^*) \cdot (\eta_1(-K)(x^*)^2y^* - r_1(A + (x^*)^2)(B - g - K + 3x^*)) - \eta_1K(x^*)^2y^* \cdot (-4A\eta_1Kx^*y^*(B - g + x^*)^2 - r_2(A + (x^*)^2)^2(B - g + x^*)^2 + B\gamma\beta K(A + (x^*)^2)^2)] \cdot [2B\eta_1^2K^2(x^*)^4(y^*)^2(A + (x^*)^2)(B - g + x^*) - (g - x^*)(r_1(A + (x^*)^2)(K - 2x^*) - \eta_1K(x^*)^2y^*) \cdot (-2A\eta_1Kx^*y^*(B - g + x^*)^2 - r_2(A + (x^*)^2)^2(B - g + x^*)^2 + B\gamma\beta K(A + (x^*)^2)^2)]$$

$$\mathcal{Q}_5 = B\eta_1K(x^*)^2(A + (x^*)^2)(g - x^*)[r_1(A + (x^*)^2)(K - 2x^*) - \eta_1K(x^*)^2y^*][y^*(A + (x^*)^2)(B - g + x^*) \cdot (\eta_1(-K)(x^*)^2y^* - r_1(A + (x^*)^2)(B - g - K + 3x^*))(-4A\eta_1Kx^*y^*(B - g + x^*)^2 - r_2(A + (x^*)^2)^2(B - g + x^*)^2 + B\gamma\beta K(A + (x^*)^2)^2) + y^*(4A\eta_1Kx^*y^*(B - g + x^*)^2 + r_2(A + (x^*)^2)^2(B - g + x^*)^2 - B\gamma\beta K(A + (x^*)^2)^2) + \eta_1K(x^*)^2(A + (x^*)^2)^2(B - g + x^*)^4(r_1(A + (x^*)^2)(K - 2x^*) - \eta_1K(x^*)^2y^*)]$$

$$\mathcal{Q}_6 = 2B\eta_1K(x^*)^2y^*(A + (x^*)^2)(g - x^*)(B - g + x^*)[r_1(A + (x^*)^2)(K - 2x^*) - \eta_1K(x^*)^2y^*] \cdot [(A + (x^*)^2)^2(B - g + x^*)(r_1(A + (x^*)^2)(B - g - K + 3x^*) + \eta_1K(x^*)^2y^*)^2 - \eta_1K^2(x^*)^2y^*(A\eta_1y^*(A - 3(x^*)^2)(B - g + x^*)^3 + B\gamma\beta(A + (x^*)^2)^3)]$$

$$\mathcal{Q}_7 = [B\eta_1^2K^2(x^*)^4(y^*)^2(A + (x^*)^2)(B - g + x^*) + (g - x^*)(r_1(A + (x^*)^2)(K - 2x^*) - \eta_1K(x^*)^2y^*) \cdot (-2A\eta_1Kx^*y^*(B - g + x^*)^2 - r_2(A + (x^*)^2)^2(B - g + x^*)^2 + B\gamma\beta K(A + (x^*)^2)^2)] \cdot [K(g - x^*)(r_1(A + (x^*)^2)(K - 2x^*) - \eta_1K(x^*)^2y^*)(2A\eta_1y^*(A - 3(x^*)^2)(B - g + x^*)^3 + B\gamma\beta(A + (x^*)^2)^3) - 2B\eta_1K(x^*)^2y^*(A + (x^*)^2)(B - g + x^*)(\eta_1Kx^*y^*(2Ax(B - g) + x^*(2Ax + A) + (x^*)^3) - r_1(A + (x^*)^2)^2(K - 2x^*)) + 3(A + (x^*)^2)^2(g - x^*)(B - g + x^*)(r_1(A + (x^*)^2)(K - 2x^*) - \eta_1K(x^*)^2y^*)^2]$$

If  $L = 0$ , then system (2.1) undergoes generalized Hopf-bifurcation. But, it is difficult to show  $L = 0$ , so the occurrence of generalized Hopf-bifurcation can be confirmed numerically for certain parametric values.  $\square$

**Theorem 6.13.** System (2.1) undergoes a Bautin (Generalized Hopf) bifurcation at the interior equilibrium point  $E_I(x^*, y^*)$  when it reaches the bifurcation threshold  $(\beta^{GH}, r_2^{GH})$ , whenever the value of  $E_I(x^*, y^*)$  meets the following requirements:

- (GH1)  $T = \text{tr}(J(E_I; (\beta^{GH}, r_2^{GH}))) = 0$
  - (GH2)  $D = \det(J(E_I; (\beta^{GH}, r_2^{GH}))) > 0$
  - (GH3)  $L(E_I; (\beta^{GH}, r_2^{GH})) = 0$
- where  $L$  is the first Lyapunov number.

*Proof.* Proceeding as in Theorem 6.12, the results can be obtained.  $\square$

**Theorem 6.14.** System (2.1) undergoes a Bautin (Generalized Hopf) bifurcation at the interior equilibrium point  $E_I(x^*, y^*)$  when it reaches the bifurcation threshold  $(r_2^{GH}, \eta_1^{GH})$ , whenever the value of  $E_I(x^*, y^*)$  meets the following requirements:

- (GH1)  $T = \text{tr}(J(E_I; (r_2^{GH}, \eta_1^{GH}))) = 0$
  - (GH2)  $D = \det(J(E_I; (r_2^{GH}, \eta_1^{GH}))) > 0$
  - (GH3)  $L(E_I; (r_2^{GH}, \eta_1^{GH})) = 0$
- where  $L$  is the first Lyapunov number.

*Proof.* It can be obtained by following Theorem 6.12.

$\square$

### 6.6. Cusp Bifurcation

We have determined that by choosing suitable parameter values, system (2.1) may possess three interior equilibrium points, which are denoted as  $E_{I1}$ ,  $E_{I2}$ , and  $E_{I3}$ . When we successively modify any parameter value, there are two potential outcomes: Either  $E_{I1}$  and  $E_{I2}$  coincide, or  $E_{I2}$  and  $E_{I3}$  coincide, leading to the occurrence of two saddle-node bifurcations. These two saddle-node bifurcation points result in two distinct saddle-node bifurcation curves within a particular two parameteric bifurcation plane. At certain parameter values, coincidence of these two saddle-node bifurcation curves leads to a cusp bifurcation [27]. In simple terms, cusp bifurcation occurs when three coexistence equilibrium points of a system come together and coincide. The lack of an explicit expression for coexistence equilibrium point makes it difficult to evaluate the coordinates of Cusp bifurcation. Thus, it is important to have numerical confirmation in order to validate the existence of this bifurcation (refer to Fig.9 & Fig.13).

## 7. Numerical simulation

For pictorial representations of local and global bifurcations, basins of attraction, and hysteresis loop, as well as to examine the influence of various parameters on the dynamical behavior of system (2.1), we conduct a series of numerical simulations in this section.

### 7.1. One-parametric bifurcation analysis

Consider a parameter in system (2.1) to examine thoroughly several bifurcation diagrams, which give us an entire understanding of how the dynamics of the system vary with respect to the chosen parameter. Let us vary the parameter  $\beta$  (grazing coefficient of filter-feeding fish) and keeping other parameter values unchanged at  $\{r_1 = 1.18, K = 4.06, g = 0.164, B = 0.27, \gamma = 0.84, r_2 = 0.61, d_1 = 0.49, \eta_1 = 0.25, A = 0.5\}$ . In this bifurcation scenario,  $E_0(0, 0)$  remains unstable for all  $\beta$ . In fig.3, we observed that one stable and one unstable coexistence equilibrium points intersect with each other and vanishes at  $\beta = \beta^{(SN_1)} = 0.82016136$ . A similar type of scenario occurs between a unstable coexistence equilibrium point and another stable coexistence equilibrium point at  $\beta = \beta^{(SN_2)} = 0.24197857$ . As a result, saddle node bifurcation occurs at  $\beta = \beta^{(SN_1)}, \beta = \beta^{(SN_2)}$ . On the other hand, the system's stability shifts when a predator-free equilibrium point  $E_a$  meets with a coexistence equilibrium point at  $\beta = \beta^{(TC)} = 0.62375941$ . At  $\beta = \beta^{(TC)}$ , a transcritical bifurcation occurs, where  $E_a$  becomes unstable and a stable coexistence equilibrium point appears. For

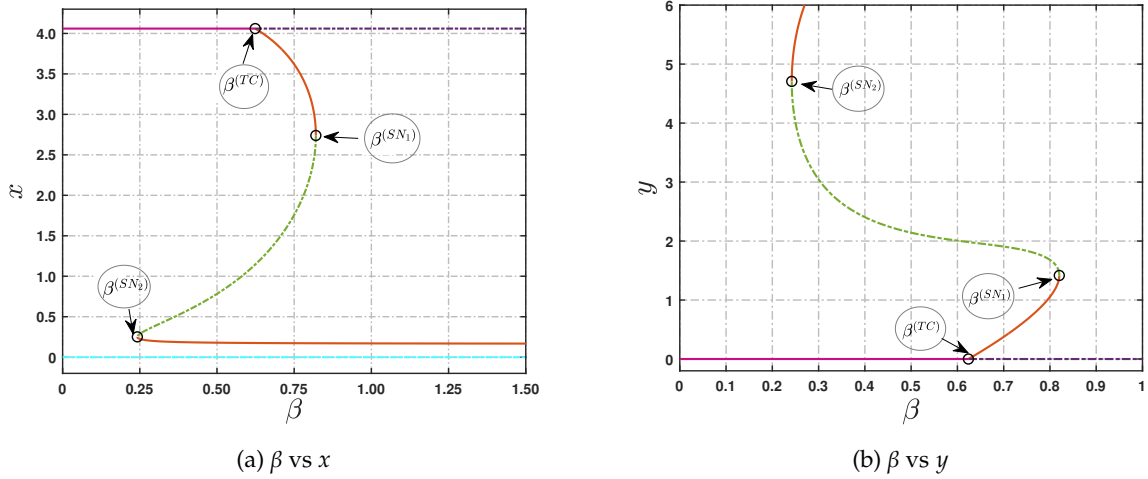


Figure 3: Bifurcation diagram of system (2.1) for the bifurcation parameter  $\beta$ . The cyan dotted and violet dotted curves indicate unstable trivial equilibrium point ( $E_0$ ) and unstable predator free equilibrium point ( $E_a$ ), respectively. The pink solid curve denotes the stable behavior of predator free equilibrium point ( $E_a$ ). The orange solid and green dotted curves represent stable and unstable behavior of the interior equilibrium point ( $E_I$ ), respectively.

Table 3: Nature of equilibrium states for the parameter range of  $\beta$ , shown in fig.(3).

Range	Equilibrium states	Nature of equilibrium states
$0 < \beta < \beta^{(SN_2)}$	$E_0, E_a$	$E_0$ is unstable and $E_a$ is LAS
$\beta^{(SN_2)} < \beta < \beta^{(TC)}$	$E_0, E_a, \text{Two interiors}$	$E_0$ is unstable, $E_a$ is LAS, one interior is unstable and another is LAS
$\beta^{(TC)} < \beta < \beta^{(SN_1)}$	$E_0, E_a, \text{Three interiors}$	$E_0$ is unstable and $E_a$ is unstable, Two interiors are LAS, one interior is unstable
$\beta > \beta^{(SN_1)}$	$E_0, E_a, \text{One interior}$	$E_0$ is unstable, $E_a$ is unstable and the interior is LAS

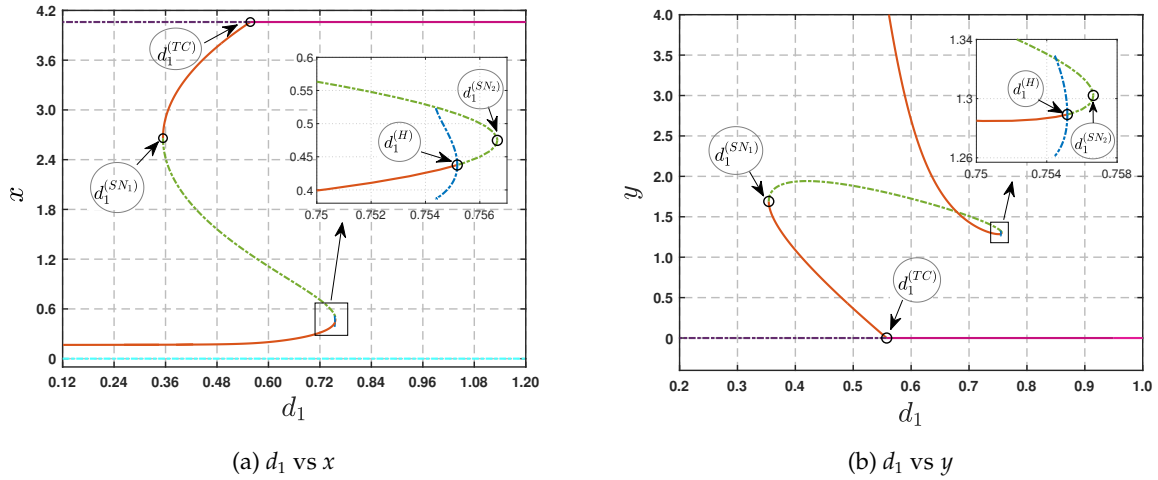


Figure 4: The bifurcation diagram illustrates the behavior of system (2.1) when the bifurcation parameter  $d_1$  varies. The cyan dotted curve represents the unstable trivial equilibrium point ( $E_0$ ), whereas the violet dotted curve represents the unstable predator free equilibrium point ( $E_a$ ). The pink solid curve represents the stable state of the predator free equilibrium point ( $E_a$ ). The orange solid and green dotted curves depict the stable and unstable characteristics of the interior equilibrium point ( $E_i$ ), respectively. The unstable limit cycle is shown by the blue dotted curve.

varying the parameter  $\beta$ , we observe some changes in number and nature of equilibrium points, which are shown in Table 3. Due to the presence of a stable predator free and a stable coexistence equilibrium point in  $\beta^{(SN_2)} < \beta < \beta^{(TC)}$ , a bi-stability phenomenon emerges. A similar type of phenomenon is observed between two stable coexistence equilibrium points in  $\beta^{(TC)} < \beta < \beta^{(SN_1)}$ .

Next we examine bifurcation parameter  $d_1$ , which indicates natural mortality rate of predator species. Initially, we fixed parameter values to  $\{r_1 = 1.18, K = 4.06, g = 0.164, B = 0.27, \gamma = 0.84, r_2 = 0.61, \beta = 0.71, \eta_1 = 0.25, A = 0.5\}$  and vary the parameter  $d_1$ . In fig.4, a coexistence equilibrium point lost its stability at  $d_1 = d_1^{(H)} = 0.75516967$ , resulting in the emergence of Hopf-bifurcation, which is subcritical due to positive lyapunov coefficient. As a result a unstable limit cycle occurs (shown in fig.5). This unstable coexistence equilibrium point approaches and collides with another unstable coexistence equilibrium point at  $d_1 = d_1^{(SN_2)} = 0.75664601$ . Additionally, a similar kind of situation is observed between one unstable and one stable coexistence equilibrium points at  $d_1 = d_1^{(SN_1)} = 0.35406954$ .

As a result, saddle node bifurcation occurs at  $d_1 = d_1^{(SN_1)}$  and  $d_1 = d_1^{(SN_2)}$ . On the other hand, a shift of stability observed between coexistence equilibrium point and  $E_a$  at  $d_1 = d_1^{(TC)} = 0.5577471$ . Consequently, at  $d_1 = d_1^{(TC)}$ , a transcritical bifurcation takes place, where  $E_a$  becomes stable and coexistence equilibrium point disappears. By varying the parameter  $d_1$ , we have seen variations in both the number and characteristics of equilibrium points. These changes are shown in Table 4. Due to presence of two stable coexistence equilibrium points in  $d_1^{(SN_1)} < d_1 < d_1^{(TC)}$ , a bi-stability phenomenon emerges. A similar type of phenomenon is observed between a coexistence and predator free equilibrium point in  $d_1^{(TC)} < d_1 < d_1^{(H)}$ .

To investigate system (2.1) in another way, let us take parameter  $r_2$ , representing intrinsic growth rate of filter-feeding fish. At first, set the parametric values at  $\{r_1 = 1.18, K = 4.06, g = 0.164, B = 0.27, \gamma = 0.84, d_1 = 0.49, \beta = 0.71, \eta_1 = 0.25, A = 0.5\}$  and vary the parameter  $r_2$ . In fig.6, one stable and one unstable coexistence stationary states are converge and collide at  $r_2 = r_2^{(SN_1)} = 1.1093139$ . Additionally, two unstable coexistence equilibrium point converge and collide with each other at  $r_2 = r_2^{(SN_2)} = 0.30632806$ . As a result, saddle node bifurcation occurs at  $r_2 = r_2^{(SN_1)}$  and  $r_2 = r_2^{(SN_2)}$ . Between these unstable coexistence

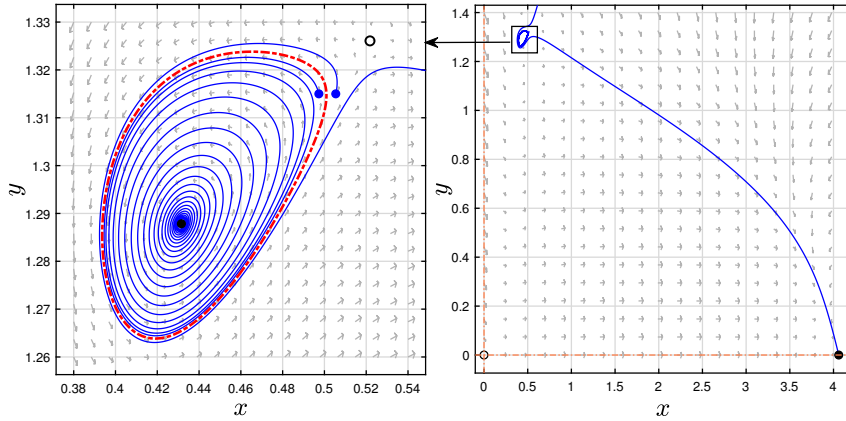


Figure 5: The phase portrait of system demonstrates the presence of a unstable limit cycle with respect to parameter  $d_1$ . The red (dotted) curve depicts unstable limit cycle, whereas blue curve reflects the paths that originate from different  $(x(0), y(0))$ , marked by solid blue dots. The black dotted point and black circular point indicate the stable and unstable equilibrium point of system (2.1) respectively.

Table 4: Nature of equilibrium states for the parameter range of  $d_1$ , shown in fig.(4).

Range	Equilibrium states	Nature of equilibrium states
$0 < d_1 < d_1^{(SN_1)}$	$E_0, E_a$ , One interior	$E_0$ is unstable, $E_a$ is unstable and the interior is LAS
$d_1^{(SN_1)} < d_1 < d_1^{(TC)}$	$E_0, E_a$ , Three interiors	$E_0$ is unstable, $E_a$ is unstable and one interior is unstable and two interiors are LAS
$d_1^{(TC)} < d_1 < d_1^{(H)}$	$E_0, E_a$ , Two interiors	$E_0$ is unstable and $E_a$ is LAS, one interior is unstable and other interior is LAS
$d_1^{(H)} < d_1 < d_1^{(SN_2)}$	$E_0, E_a$ , Two interiors	$E_0$ is unstable, $E_a$ is LAS and both interiors are unstable
$d_1 > d_1^{(SN_2)}$	$E_0, E_a$	$E_0$ is unstable, $E_a$ is LAS

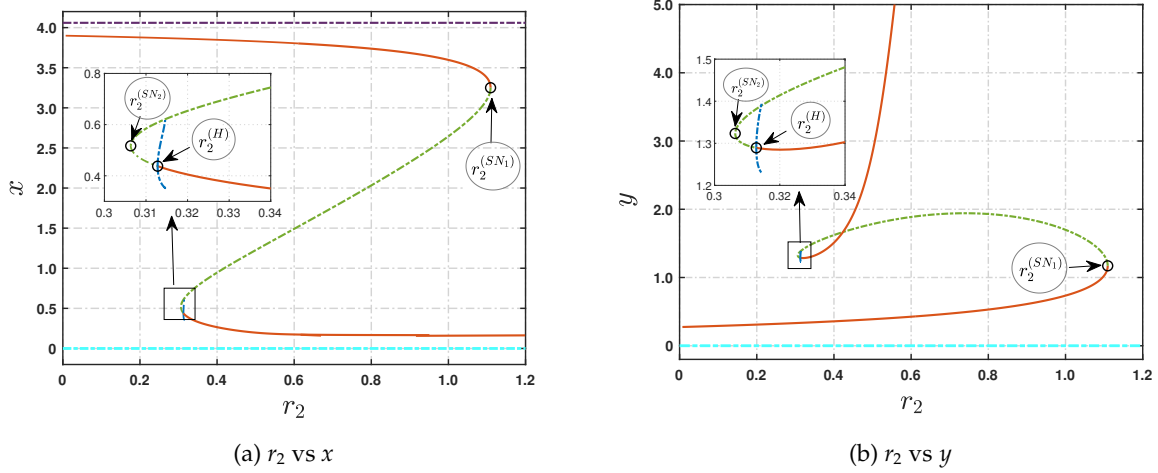


Figure 6: The bifurcation diagram shows the behavior of system (2.1) when the bifurcation parameter  $r_2$  changes. The cyan dotted curve represents the unstable trivial equilibrium point ( $E_0$ ), while the violet dotted curve indicates the unstable predator free equilibrium point ( $E_H$ ). The orange solid and green dotted curves represent the stable and unstable behavior of coexistence stationary state ( $E_I$ ), respectively. Blue dotted curve denotes unstable limit cycle.

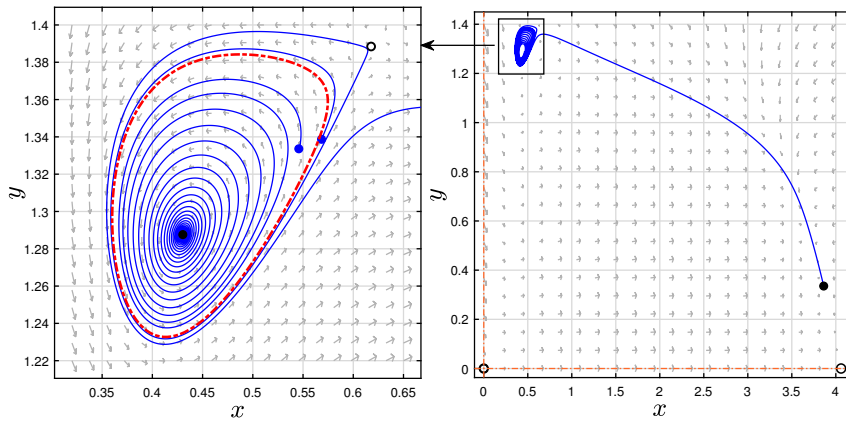


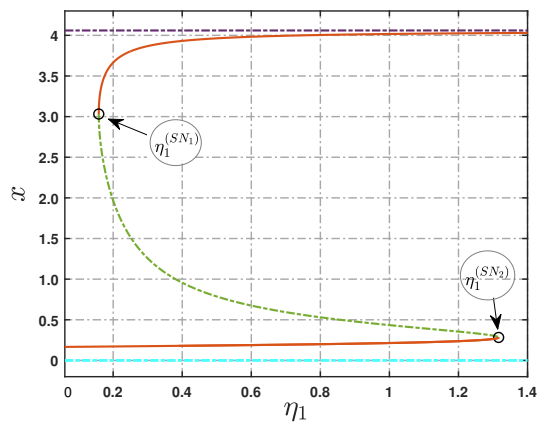
Figure 7: The phase portrait shows the presence of unstable limit cycle with respect to the parameter  $r_2$ . The red dotted curve represents unstable limit cycle, whereas the blue curve shows the trajectory that starts from different  $(x(0), y(0))$ , shown by solid blue dots. The black dot reflects the stable equilibrium points, whereas the black circle denotes the unstable equilibrium point in system (2.1).

stationary states, one unstable coexistence stationary state gains its stability at  $r_2 = r_2^{(H)} = 0.31279657$ , resulting in an appearance of Hopf-bifurcation, which is subcritical due to positive Lyapunov coefficient. As a result a unstable limit cycle occurs (shown in fig.7). Through experimentation with different values of parameter  $r_2$ , we have observed changes in both the number and behavior of stability of the equilibrium points. The changes are provided in Table 5. The presence of two stable coexistence equilibrium points in  $r_2^{(H)} < r_2 < r_2^{(SN_1)}$ , results in a bi-stability phenomenon.

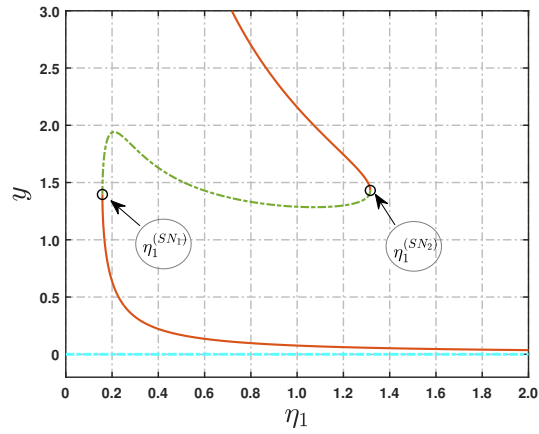
For more experiments, we have also varied parameter  $\eta_1$ , the toxicity coefficient of predator population and kept other remaining parameters fixed at  $\{r_1 = 1.18, K = 4.06, \beta = 0.71, g = 0.164, B = 0.27, \gamma = 0.84, r_2 = 0.61, d_1 = 0.49, A = 0.5\}$ . In fig.8, we have noticed a convergence and collision between a stable and an unstable coexistence equilibrium point at a certain value of  $\eta_1 = 0.15825935$ , denoted as  $\eta_1^{(SN_1)}$ .

Table 5: Nature of equilibrium states for the parameter range of  $r_2$ , shown in fig.(6).

Range	Equilibrium states	Nature of equilibrium states
$0 < r_2 < r_2^{(SN_2)}$	$E_0, E_a$ , One interior	$E_0$ is unstable and $E_a$ is unstable and the interior is LAS
$r_2^{(SN_2)} < r_2 < r_2^{(H)}$	$E_0, E_a$ , Three interiors	$E_0$ is unstable, $E_a$ is unstable and one interior is LAS and two interiors are unstable
$r_2^{(H)} < r_2 < r_2^{(SN_1)}$	$E_0, E_a$ , Three interiors	$E_0$ is unstable and $E_a$ is unstable, one interior is unstable and other two interiors are LAS
$r_2 > r_2^{(SN_1)}$	$E_0, E_a$ , One interior	$E_0$ is unstable, $E_a$ is unstable and the interior is LAS



(a)  $\eta_1$  vs  $x$



(b)  $\eta_1$  vs  $y$

Figure 8: The bifurcation diagram illustrates the dynamics of system (2.1) as the bifurcation parameter  $\eta_1$  varies. The cyan dotted curve indicates the unstable trivial equilibrium point ( $E_0$ ), whereas the violet dotted curve indicates the unstable predator free equilibrium point ( $E_a$ ). The orange solid and green dotted curves depict the stable and unstable characteristics of the coexistence stationary state ( $E_I$ ), respectively.

Table 6: Nature of equilibrium states for the parameter range of  $\eta_1$ , shown in fig.8.

Range	Equilibrium states	Nature of equilibrium states
$0 < \eta_1 < \eta_1^{(SN_1)}$	$E_0, E_a$ , One interior	$E_0$ is unstable and $E_a$ is unstable and the interior is LAS
$\eta_1^{(SN_1)} < \eta_1 < \eta_1^{(SN_2)}$	$E_0, E_a$ , Three interiors	$E_0$ is unstable, $E_a$ is unstable and one interior is unstable and two interiors are LAS
$\eta_1 > \eta_1^{(SN_2)}$	$E_0, E_a$ , One interior	$E_0$ is unstable, $E_a$ is unstable and the interior is LAS

Additionally, a similar type of scenario occurs between a stable and a unstable coexistence equilibrium point at  $\eta_1 = \eta_1^{(SN_2)} = 1.3162526$ . As a consequence, saddle node bifurcation occurs at  $\eta_1 = \eta_1^{(SN_1)}$  and  $\eta_1 = \eta_1^{(SN_2)}$ .

Through the process of conducting experiments with varying values of the parameter  $\eta_1$ , we have noticed variations in the number of equilibrium points and the stability characteristics of those points, which is provided in Table 6. Due to presence of two stable coexistence stationary states in  $\eta_1^{(SN_1)} < \eta_1 < \eta_1^{(SN_2)}$ , a bi-stability phenomenon emerges.

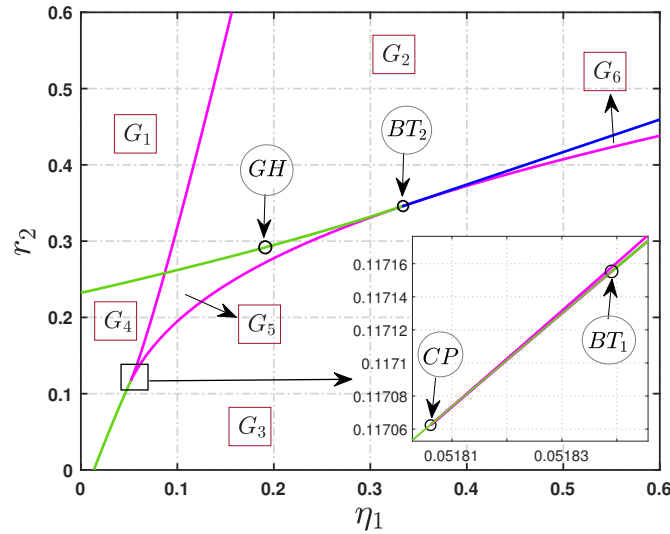


Figure 9: In the  $\eta_1 - r_2$  plane, there is a two-parameter bifurcation diagram of system (2.1). The solid pink curve indicates saddle-node bifurcation curve for coexistence stationary state. Here, solid green curve indicates Hopf-bifurcation curve, while the solid blue curve represents the homoclinic bifurcation curve for coexistence equilibrium point.

### 7.2. Two-parametric bifurcation analysis

Let us, examine bifurcation diagrams by changing two parameters in system (2.1). This analysis provides a comprehensive understanding of how the dynamics of system is affected by variations in chosen parameter. We select toxicity coefficient of predator population  $\eta_1$  and intrinsic growth rate of filter-feeding fish (predator)  $r_2$  as the key parameters for studying system (2.1). So, we generate two-parametric bifurcation diagram in  $\eta_1 - r_2$  plane, while keeping remaining parameters at  $\{r_1 = 1.18, K = 4.06, \beta = 0.71, g = 0.164, B = 0.27, \gamma = 0.84, d_1 = 0.49, A = 0.5\}$ , which is shown in fig.9. Fig.9 includes two Hopf-bifurcation curves (green), two saddle-node bifurcation curves (pink) and one homoclinic curve (blue). These bifurcation curves divide entire  $\eta_1 - r_2$  parametric plane into six separate regions, i.e.,  $G_1, G_2, G_3, G_4, G_5$  and  $G_6$ . These regions will be examined in more depth in the following discussion, which is presented below. Several co-dimension 2 bifurcation points appear when these bifurcation curves come together. A cusp bifurcation, which arises at  $CP(0.051806132, 0.11706239)$ , is one such occurrence, where two saddle-node bifurcation curves meet and then disappear. On the other hand, Hopf-bifurcation curve meets with saddle node bifurcation curve at  $BT_1(0.051839047, 0.11715533)$  and Hopf-bifurcation curve disappears. As a result, Bogdanov–Takens bifurcation occurs at this point. There is another Hopf-bifurcation curve that includes a generalized Hopf-bifurcation point at coordinates  $GH(0.19111678, 0.29187368)$ , where the supercritical Hopf-bifurcation undergoes a transition to subcritical Hopf-bifurcation. Moreover, this Hopf-bifurcation curve touches saddle–node bifurcation curve tangentially at  $BT_2(0.33392155, 0.34597642)$ . As a result, the Bogdanov-Takens bifurcation takes place at this specific position, causing the disappearance of the Hopf-bifurcation curve. Furthermore, the homoclinic bifurcation curve originates from this Bogdanov-Takens bifurcation point. On this bifurcation curve, a unique closed orbit is produced, establishing a link between a saddle coexistence equilibrium point and itself. The closed orbit seen in Figure 10 is known as homoclinic orbit.

Our next step is to take a closer look at the unique dynamic characteristics of every region. In region  $G_1$ , the system has one unstable trivial, one unstable predator free and one stable coexistence equilibrium points. When a transition takes place from  $G_1$  to  $G_2$ , a saddle node bifurcation curve causes the emergence of two coexisting stationary states, one of which is stable and the other is unstable. Transitioning from region  $G_1$  to  $G_4$ : the stable coexistence equilibrium point lost it’s stability through Hopf-bifurcation curve. One stable and one unstable coexistence equilibrium points appear through saddle-node bifurcation curve

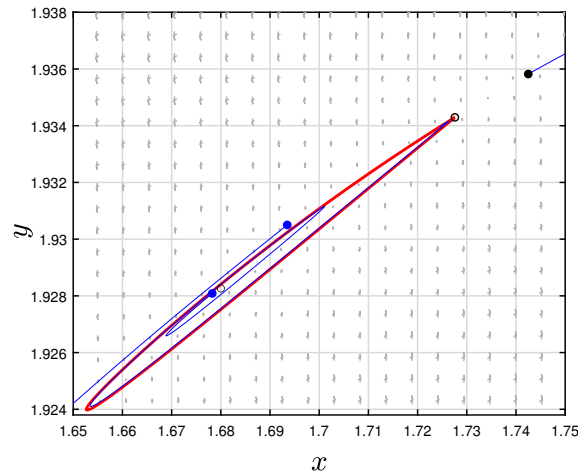


Figure 10: Evidence of existence of homoclinic bifurcation. The red solid curve depicts the homoclinic orbit, whereas the blue curve shows the trajectories that start from different  $(x(0), y(0))$ , denoted by blue dots. The black dotted point and black circular point indicates the stable and the unstable behavior of interior stationary states respectively of system (2.1).

Table 7: Nature of equilibrium states for individual regions of  $\eta_1$  vs  $r_2$  bifurcation, shown in fig.9.

Regions	Equilibrium states	Nature of equilibrium states
$G_1$	$E_0, E_a$ , One interior	$E_0$ is unstable, $E_a$ is unstable and the interior is LAS
$G_2$	$E_0, E_a$ , Three interiors	$E_0$ is unstable, $E_a$ is unstable, two interiors are LAS and One interior is unstable
$G_3$	$E_0, E_a$ , One interior	$E_0$ is unstable, $E_a$ is unstable and the interior is LAS
$G_4$	$E_0, E_a$ , One interior	$E_0$ is unstable, $E_a$ is unstable and The interior is unstable spiral
$G_5$	$E_0, E_a$ , Three interiors	$E_0$ is unstable, $E_a$ is unstable, One interior is unstable, another one interior is unstable spiral and one interior is LAS
$G_6$	$E_0, E_a$ , Three interiors	$E_0$ is unstable, $E_a$ is unstable, One interior is LAS, one interior is stable spiral and other is unstable

as we enter from  $G_4$  to  $G_5$ . Moving from region  $G_5$  to  $G_3$ , two coexistence equilibrium points disappear through saddle-node bifurcation curve. Finally, when we transit from  $G_3$  to  $G_6$ , a saddle-node bifurcation curve gives rise to two coexistence equilibrium points, one of which is stable and the other is unstable. To facilitate all the characteristics of equilibrium points of each regions in  $\eta_1 - r_2$  parametric plane, 7 is displayed.

Our current objective is to create phase portraits of (2.1). In order to achieve this, we choose  $\eta_1$  and  $r_2$  from each region, fixing other parameter values at  $\{r_1 = 1.18, K = 4.06, \beta = 0.71, g = 0.164, B = 0.27, \gamma = 0.84, d_1 = 0.49, A = 0.5\}$ . The phase portraits are shown in Fig.11. After analyzing these phase portraits, it is evident that the presence of two stable coexistence equilibrium points inside the regions  $G_2$  and  $G_6$  lead to a bi-stable phenomenon. Under such conditions, each species' population size depends on their respective initial population size. Moreover, the system has only one stable coexistence equilibrium point in each of the regions  $G_1, G_3$  and  $G_6$ . In this scenario, both species' populations stay a steady state whatever their initial population size. Population biomass of both species oscillates around coexistence equilibrium point inside  $G_4$ .

To investigate system (2.1) from an other perspective, let us choose  $r_2$  (intrinsic growth rate of filter-feeding fish) and  $\beta$  (grazing coefficient of filter-feeding fish) for further analysis. Presently, we create two-parametric

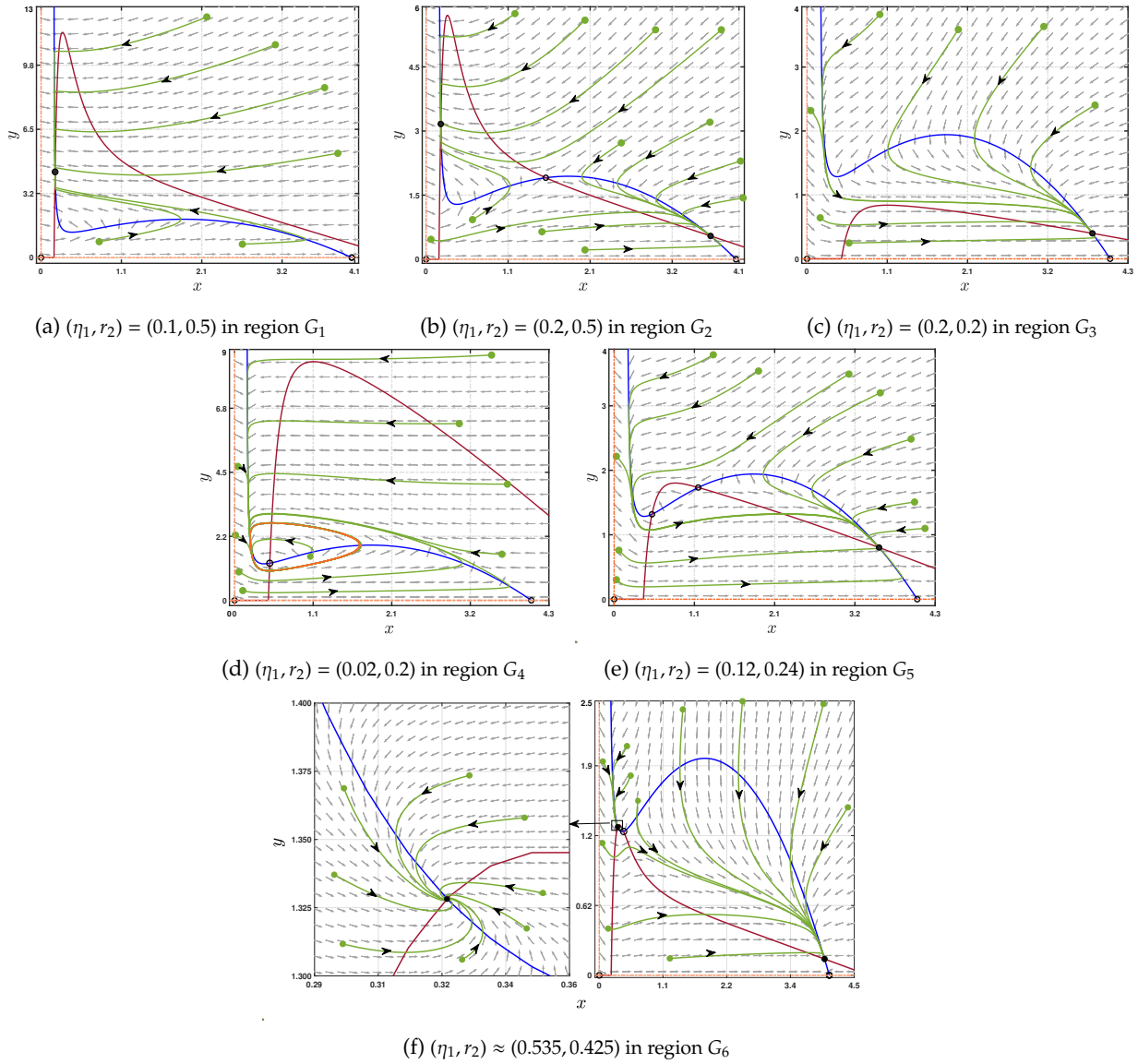


Figure 11: Phase portrait of (2.1) for regions  $G_1, G_2, G_3, G_4, G_5$  and  $G_6$  as mentioned in fig.9. The red solid curve represents the predator nullcline, whereas the blue solid curve represents the prey nullcline. The green solid curves show the paths start from different  $(x(0), y(0))$ , indicated by green dots. The black dotted point and black circular point indicates the stable and unstable characteristic of stationary states of (2.1) respectively. The vector field has been shown in each figure.

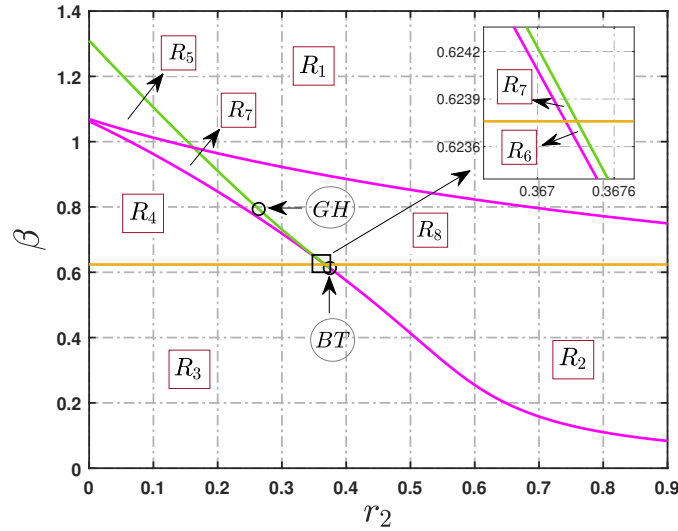


Figure 12: Bifurcation diagram of system (2.1) in two-parametric plane  $r_2 - \beta$ . Here, pink solid curve depicts saddle node bifurcation curve of coexistence equilibrium point, while green curve (solid) denotes Hopf-bifurcation curve, and yellow solid curve indicates transcritical bifurcation curve.

bifurcation diagram in  $r_2 - \beta$  plane, while maintaining all other parameters at  $\{r_1 = 1.18, K = 4.06, g = 0.164, B = 0.27, \gamma = 0.84, d_1 = 0.49, \eta_1 = 0.25, A = 0.5\}$ . Fig.12 represents corresponding bifurcation diagram, which contains one Hopf-bifurcation curve (green), two saddle-node bifurcation curves (pink) and one transcritical bifurcation curve (yellow). These bifurcation curves divide the whole parametric plane  $r_2 - \beta$  into eight distinct regions, namely  $R_1, R_2, R_3, R_4, R_5, R_6, R_7$  and  $R_8$ . The subsequent discussion will provide a more comprehensive analysis of these regions. It is noticed that the Hopf-bifurcation curve includes a generalized Hopf-bifurcation point, at coordinates  $GH(0.2638859, 0.79380602)$ , where a transition takes place from supercritical Hopf-bifurcation to subcritical Hopf-bifurcation. Moreover, this Hopf-bifurcation curve meets tangentially with saddle node bifurcation curve at  $BT(0.37455134, 0.61295545)$ , after that the Hopf-bifurcation curve disappears. As a result, Bogdanov-Taken bifurcation occurs at this point, which is a codimension 2 bifurcation.

Now, let's delve into the distinct dynamic attributes of each region separately. In region  $R_1$ , the system has one unstable trivial, one unstable predator free and one stable coexistence stationary state. As we move from  $R_1$  to  $R_8$ , saddle node bifurcation curve leads to two coexistence equilibrium states between which one is stable and other is unstable. On the other hand, moving from region  $R_1$  to region  $R_5$ , stable coexistence equilibrium point lost its stability as it crosses Hopf-bifurcation curve. When we shift from region  $R_8$  to  $R_2$ , the unstable predator free equilibrium point becomes stable and the stable coexistence equilibrium point disappears through transcritical bifurcation curve. If transition takes place from region  $R_2$  to  $R_3$ , two coexistence equilibrium points disappear because of crossing saddle node bifurcation curve. Moreover, Shifting from  $R_3$  to  $R_4$ ,  $E_a$  becomes unstable and one stable coexistence equilibrium point arises through transcritical bifurcation curve. While moving from  $R_2$  to  $R_6$ , one coexistence equilibrium point lost its stability through Hopf-bifurcation curve. Furthermore, shifting from  $R_4$  to  $R_7$ , saddle node bifurcation curve leads to two coexistence equilibrium points, both are unstable. In Table 8, the stability behavior of all equilibrium points in each region of the  $r_2 - \beta$  parametric plane are provided.

For further examination of our proposed system (2.1), we have taken the parameters  $d_1$  (natural mortality rate of predator) and  $\beta$  (grazing coefficient of filter-feeding fish). Two-parametric bifurcation diagrams in  $d_1 - \beta$  plane while keeping remaining parameters at  $\{r_1 = 1.18, K = 4.06, g = 0.164, B = 0.27, \gamma = 0.84, r_2 = 0.61, \eta_1 = 0.25, A = 0.5\}$  are depicted. Fig.13 represents the corresponding bifurcation diagram, which contains several bifurcation curves. There are two Hopf-bifurcation curves in green, two saddle-node

Table 8: Nature of equilibrium states for each regions of  $r_2$  vs  $\beta$  bifurcation, shown in fig.(12).

Regions	Equilibrium states	Nature of equilibrium states
$R_1$	$E_0, E_a$ , One interior	$E_0$ is unstable, $E_a$ is unstable and the interior is LAS
$R_2$	$E_0, E_a$ , Two interiors	$E_0$ is unstable, $E_a$ is LAS, one interior is unstable and another one interior is LAS
$R_3$	$E_0, E_a$	$E_0$ is unstable and $E_a$ is LAS
$R_4$	$E_0, E_a$ , One interior	$E_0$ is unstable, $E_a$ is unstable and the interior is LAS
$R_5$	$E_0, E_a$ , One interior	$E_0$ is unstable, $E_a$ is unstable, One interior is unstable spiral
$R_6$	$E_0, E_a$ , Two interiors	$E_0$ is unstable, $E_a$ is LAS, One interior is unstable and another one interior is unstable spiral
$R_7$	$E_0, E_a$ , Three interiors	$E_0$ is unstable, $E_a$ is unstable, One interior is unstable, another interior is unstable spiral and the third interior is LAS
$R_8$	$E_0, E_a$ , Three interiors	$E_0$ is unstable, $E_a$ is unstable, Two interiors are LAS and one interior is unstable.

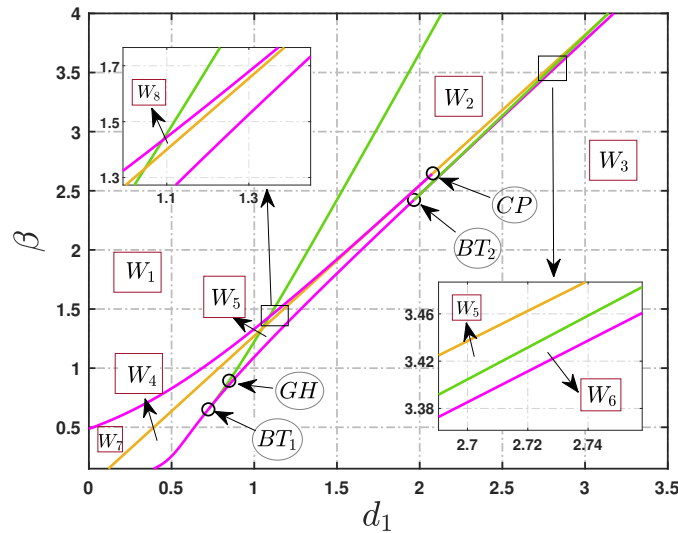


Figure 13: Two-parametric bifurcation diagram on the  $d_1 - \beta$  plane. The pink solid curve shows saddle-node bifurcation curve for the coexistence stationary state. The green curve (solid) illustrates Hopf-bifurcation curve, while the yellow curve (solid) indicates the transcritical bifurcation curve.

bifurcation curves in pink, a transcritical bifurcation curve in yellow. These bifurcation curves splitting the whole parametric plane  $d_1 - \beta$  into eight separate regions:  $W_1, W_2, W_3, W_4, W_5, W_6, W_7$  and  $W_8$ . A generalized Hopf-bifurcation is observed at  $GH(0.84855546, 0.89350739)$  on the Hopf-bifurcation curve, where supercritical Hopf-bifurcation transits to subcritical Hopf-bifurcation. At  $BT_1(0.72244603, 0.65150641)$ , this Hopf-bifurcation curve meets with saddle-node bifurcation curve tangentially and vanishes. At  $BT_1$ , Bogdanov-Takens bifurcation occurs. Again, another Hopf-bifurcation curve touches saddle node bifurcation curve at  $BT_2(1.9656289, 2.4231606)$ . Consequently, the Bogdanov-Takens bifurcation occurs at this specific point, causing the Hopf-bifurcation curve to disappear. Furthermore, we have found a cusp bifurcation point at  $CP(2.0795238, 2.6471889)$ , where saddle node bifurcation curve intersects transcritical bifurcation curve and the saddle node curve vanishes. Next we observe changes of stability behavior and number of equilibrium points in different regions of this parametric plane. The change of stability of all equilibrium points in each region of the parametric plane  $d_1 - \beta$  are shown in Table 9.

Table 9: Nature of equilibrium states for each regions of  $d_1$  vs  $\beta$  bifurcation, shown in fig.(13).

Regions	Equilibrium states	Nature of equilibrium states
$W_1$	$E_0, E_a$ , One interior	$E_0$ is unstable, $E_a$ is unstable and the interior is LAS
$W_2$	$E_0, E_a$ , One interior	$E_0$ is unstable, $E_a$ is unstable and the interior is unstable spiral
$W_3$	$E_0, E_a$	$E_0$ is unstable and $E_a$ is LAS
$W_4$	$E_0, E_a$ , Two interiors	$E_0$ is unstable, $E_a$ is LAS, one interior is unstable and other interior is LAS
$W_5$	$E_0, E_a$ , Two interiors	$E_0$ is unstable, $E_a$ is LAS, One interior is unstable and other interior is unstable spiral
$W_6$	$E_0, E_a$ , Two interiors	$E_0$ is unstable, $E_a$ is LAS, One interior is unstable and another one interior is stable spiral
$W_7$	$E_0, E_a$ , Three interiors	$E_0$ is unstable, $E_a$ is unstable, One interior is unstable, two interiors are LAS
$W_8$	$E_0, E_a$ , Three interiors	$E_0$ is unstable, $E_a$ is unstable, One interior is unstable, another one interior is unstable spiral and other interior is LAS

### 7.3. Evidence of bi-stable phenomenon and basins of attraction

While examining our system (2.1), we have found a looping behavior in prey population due to fluctuations in toxicity coefficient of predator population  $\eta_1$  and intrinsic growth rate of filter-feeding fish  $r_2$ , which are shown in fig.14. In this diagram, the solid orange curve denotes the stable behavior of coexistence equilibrium point and green curve (dotted) is representing unstable behavior of coexistence equilibrium point. In fig.14a, within the shaded area, system (2.1) exhibits a saddle-node bifurcations at the points  $\eta_1^{(SN_1)}$  and  $\eta_1^{(SN_2)}$  and in fig.14b, the system exhibits two saddle-node bifurcations at  $r_2 = r_2^{(SN_1)}$  and Hopf-bifurcation occurs at  $r_2^{(H)}$ . These points are located on the boundary of the shaded region. In fig.14a, we observe that the stable coexistence equilibrium point converge and collide with an unstable coexistence equilibrium point at  $\eta_1 = \eta_1^{(SN_1)}$ , results in the disappearance of both equilibrium points. Subsequently, the trajectory of system (2.1) must abruptly shift to the closest attractor of (2.1), which is another coexistence equilibrium state. In order to return to the first coexistence equilibrium state, it is necessary to invert the value of  $\eta_1$ . So, the 2<sup>nd</sup> stable coexistence equilibrium state is then followed and traversed backwards. Consequently, the system’s trajectories abruptly shift towards the 1<sup>st</sup> interior equilibrium state when the 2<sup>nd</sup> stable coexistence equilibrium state collides with unstable coexistence equilibrium state, causing them to vanish due to a saddle-node bifurcation occurring at  $\eta_1 = \eta_1^{(SN_1)}$ . Thus a looping behavior is exhibited because of the variation of  $\eta_1$ .

The similar incident happens in the prey biomass for fluctuation of parameter  $r_2$  (intrinsic growth rate of filter-feeding fish (predator)), shown in fig.14b. This phenomenon is called hysteresis. Also it is the evidence that system (2.1) has bi-stable phenomenon.

The basins of attraction refers to the collection of initial conditions that steers the system towards a certain equilibrium state over a long span of time. In simple words, it refers to the region in the state space where the behavior of the system results in a specific outcome. A comprehensive understanding of the basins of attraction is crucial for determining the enduring behavior of the system. In order to illustrate the basins of attraction for system (2.1), we setup the parametric values as:  $\{r_1 = 1.18, K = 4.06, \beta = 0.71, g = 0.164, B = 0.27, \gamma = 0.84, r_2 = 0.61, d_1 = 0.49, \eta_1 = 0.25, A = 0.5\}$ . Within this particular set of parameters, system (2.1) exhibits three coexistence equilibrium states: among which one is unstable, while the other two are LAS. Hence, a bi-stable behavior occurring between the two stable coexistence states. Associated basins of attraction is shown in Figure 15. It demonstrates that in the blue zone, population trajectories converge towards a coexistence equilibrium state characterized by a lower equilibrium biomass of *Microcystis aeruginosa* (prey). Conversely, in the green region, population trajectories trend towards a coexistence equilibrium state with a larger equilibrium biomass of prey. Therefore, when the value of  $g$

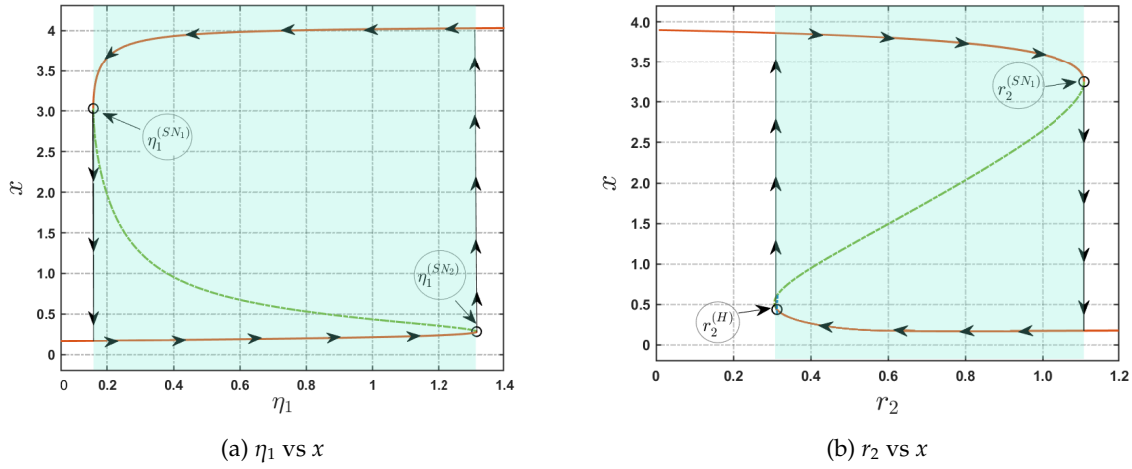


Figure 14: Diagram of the hysteresis phenomenon. The black arrows are used to demonstrate the hysteresis loop in the prey biomass inside the green shaded zone. This loop is caused by changes in the coefficient of toxicity ( $\eta_1$ ) and the intrinsic growth rate of the predator species ( $r_2$ ). The green shaded zone illustrates the occurrence of bi-stability between two coexistence equilibrium states of (2.1).

(coefficient of *Microcystis aeruginosa* aggregation) is 0.268, it is very probable that the population would reach a stable coexistence condition with a larger equilibrium biomass. In order to examine changes in the basins of attraction, we will systematically reduce the amount of aggregation. As the value of  $g$  reduces to  $g = 0.164$  and  $g = 0.02$ , the size of the blue shaded region increases, resulting in a proportional reduction in the area of the green shaded region, as shown in fig.15b and fig.15c correspondingly. It suggests that even while the filter-feeding fish population increases and reaches a higher equilibrium biomass as the value of  $g$  decreases, the chance of achieving the associated higher coexistence stationary state decreases. This happens because of strong effect of toxins. When there are more predators initially, poisoning has a strong negative effect on those species, and the effect is directly related to the number of predators. This keeps the lower coexistence stationary state stable. These results are intricate and non-intuitive, and they cannot be explicitly deduced through a straightforward investigation.

## 8. Discussion

Nowadays, toxic algal blooms and their effects on aquatic life are becoming more concerning. According to the National Oceanic and Atmospheric Administration (NOAA) and the Washington State Department of Health, toxic algal blooms, such as Florida’s red tide and Pacific Northwest shellfish poisoning, have a detrimental effect on filter-feeding creatures such as manatees and shellfish. These blossoms generate neurotoxins that harm marine organisms and the creatures which consume these algae. This emphasizes on the ecological vulnerability and economic consequences in coastal areas. Also, Nile tilapia, which are filter feeders, have been impacted by cyanobacterial blooms in Lake Victoria, by accumulating microcystins in their tissues [26]. Our research introduces a new mathematical model for aquatic ecology, specifically focusing on the impact of toxin-producing *Microcystis aeruginosa* on the dynamic interaction between *Microcystis aeruginosa* and filter-feeding fish. The model is developed using the framework of biological theory to improve the clarity of this interaction.

Initially, we have verified the well-posedness of our proposed model by showing that solutions remain positive and bounded in the region  $\Omega \subseteq \mathbb{R}_+^2$ . Afterwards, we have examined the local dynamics of proposed system (2.1). The system has one predator-free equilibrium point  $E_a$  whose stability depends on a parametric condition, which has been discussed in theorem 5.2 along with an unstable trivial equilibrium point  $E_0$ . Additionally, the system has interior equilibrium points, the number and existence of which are

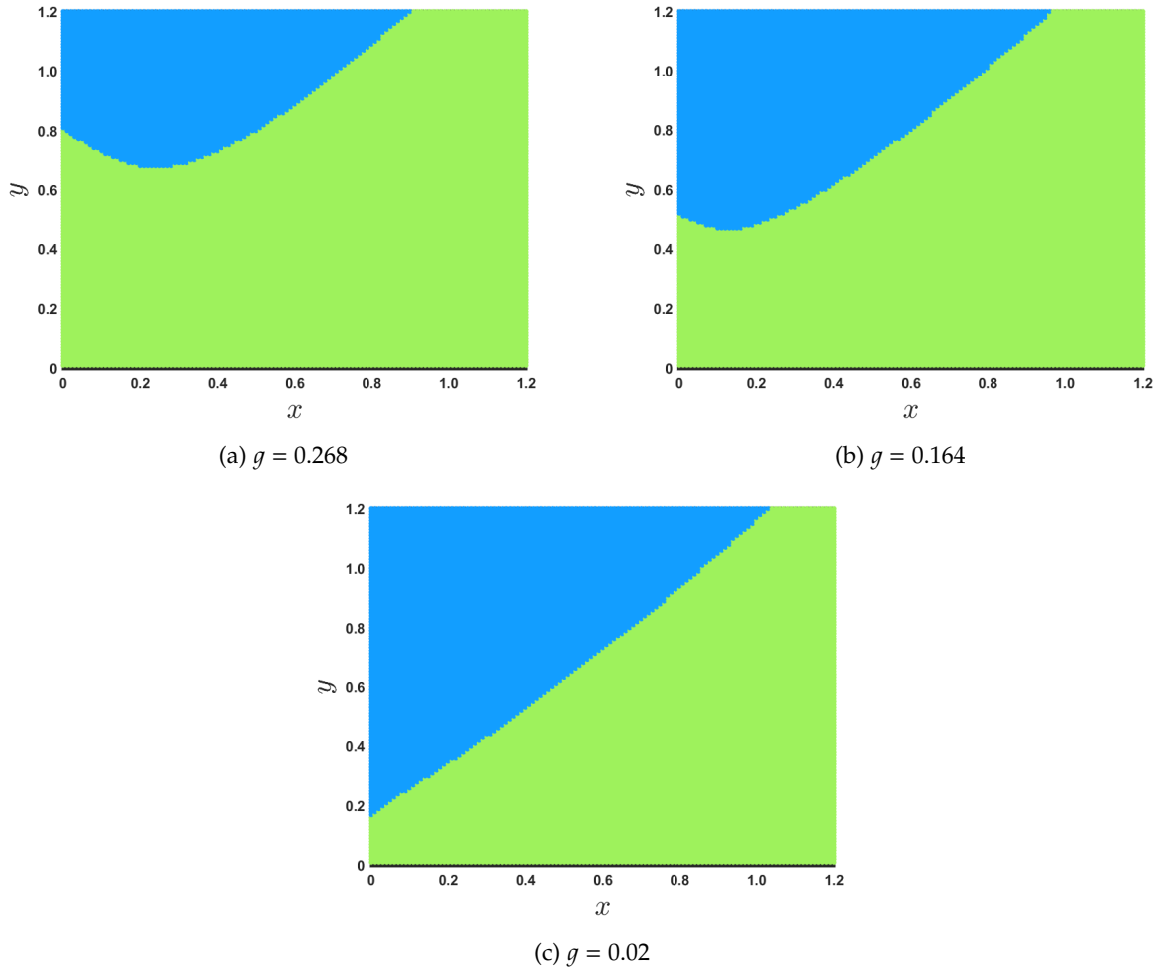


Figure 15: Basins of attraction of system (2.1) corresponding to aggregation parametric values  $g = 0.268$ ,  $g = 0.164$  and  $g = 0.02$  in Fig.15a, 15b and 15c respectively. Blue region and green region denotes the basins of attraction for two coexistence stationary states respectively.

determined by several types of factors described in section 4.2. Theorem 5.3 determines the stability behavior of coexistence stationary states. The primary focus of the present work is on two crucial factors: grazing coefficient of filter-feeding fish  $\beta$  and toxicity coefficient of predator population  $\eta_1$ . In addition, we have also included intrinsic growth rate of filter-feeding fish (predator)  $r_2$  and its natural mortality rate  $d_1$ . Then we have analyzed how the fluctuations of parameters  $\beta$ ,  $\eta_1$ ,  $r_2$  and  $d_1$  impact on system dynamics. It is shown by numerical analysis that the system undergoes one transcritical bifurcation for the parameters  $\beta$  and  $d_1$ , and two saddle-node bifurcations for the parameters  $\beta$ ,  $\eta_1$ ,  $r_2$ , and  $d_1$ . Moreover, the system undergoes one subcritical Hopf-bifurcation for the parameters  $r_2$  and  $d_1$  from which unstable bifurcating limit cycle emerges. Under certain parametric values, the system exhibits a bi-stable phenomena characterized by the presence of two interior equilibrium points. Sometimes, a bi-stable phenomena may arise between an interior and predator free equilibrium points. Also, in  $\eta_1 - r_2$  and  $d_1 - \beta$  parametric planes Bogdanov-Takens bifurcation, Generalized Hopf-bifurcation and Cusp bifurcation are occurred. Additionally, the  $\eta_1 - r_2$  parametric plane exhibits homoclinic bifurcation. Another two-parametric bifurcation diagram has also been discussed in  $r_2 - \beta$  plane, which demonstrates Bogdanov-Takens bifurcation and Generalized Hopf-bifurcation. By applying necessary mathematical theory [27], we have also derived the conditions for these bifurcations. Furthermore, the system promotes the idea of a basins of attraction as a result of the existence of bistable phenomena. As we have varied the coefficient of *Microcystis aeruginosa* aggregation  $g$ , a change in the behavior of the proposed system has been reported. The phenomena has been explained in section 7.3 using the idea of basins of attraction. Additionally, a hysteresis loop has been observed in the prey species (*Microcystis aeruginosa*) due to the variations in toxicity coefficient  $\eta_1$  of the predator (filter-feeding fish) population and its intrinsic growth rate. All of these bifurcation parameters influence the population biomass of both species. For example, when the grazing activity of filter feeding fish (predator) is low, it creates a more favorable environment for the survival of *Microcystis aeruginosa* (prey). However, prey biomass falls and predator biomass rises when grazing increases slowly. Nonetheless, significant grazing levels make it harder for prey biomass to survive, as the predator reduces the biomass of prey. It is unexpected that higher grazing levels of predator could have a negative impact on ecological diversity. This outcome is also non-intuitive, as one might expect that higher grazing levels would create an ecosystem more suitable for predator species' existence. The existence of toxicity in predator species is the main reason for this phenomenon. With a high grazing level, consumption of harmful prey is also high, which further influences the predator biomass. Although, when the natural death rate of predator species is low, it becomes more challenging for prey biomass to survive. Moreover, the rise in the natural mortality rate of predator enhances an environment for the existence of prey species. Consequently, the biomass of predators diminishes. A thorough examination of this particular model may provide us with a comprehensive understanding of how populations undergo changes in the actual world. In the upcoming future, the system may be developed to a system including two prey species and one predator species. This modification would have significant advantages in conserving biodiversity and maintaining community structure.

## Funding

This research received no external funding.

## Conflict of Interest

With reference to this study, the authors claim that they do not have any conflict of interest.

## Author contributions

All the authors have participated equally in all the aspects of this paper: conceptualization, methodology, investigation, formal analysis, writing-original draft preparation, writing-review and editing.

### Availability of data and materials

The data used to support the findings of the study are available within the article.

### Code availability

The authors have used their own code.

### Acknowledgements

The first author (Parvez Akhtar) is thankful to the University Grants Commission, Government of India for providing SRF, the second author (Souvick Karmakar) is thankful to the Ministry of Social Justice and Empowerment, Government of India for providing Fellowship, and the third author (Nirmalya Mondal) is thankful to the Council of Scientific & Industrial Research, India for providing JRF.

### References

- [1] R. P. Agarwal, O. Bazighifan, and M. A. Ragusa, *Nonlinear neutral delay differential equations of fourth-order: oscillation of solutions*, Entropy, 23(2):129, 2021.
- [2] X. Li, H. Yu, C. Dai, Z. Ma, Q. Wang, M. Zhao, *Bifurcation analysis of a new aquatic ecological model with aggregation effect* Mathematics and Computers in Simulation 90 75–96. 2021.
- [3] X. Liu, X. Lu, Y. Chen, *The effects of temperature and nutrient ratios on Microcystis blooms in Lake Taihu, China: An 11-year investigation*, Harmful algae, 0 (3) 337–343. 2011.
- [4] M. Detto, H. C. Muller-Landau, *Stabilization of species coexistence in spatial models through the aggregation–segregation effect generated by local dispersal and nonspecific local interactions*, Theoretical Population Biology, 12 97–108. 2016.
- [5] S. Pereira, A. Zille, E. Micheletti, P. Moradas-Ferreira, R. D. Philippis, P. Tamagnini, *Complexity of cyanobacterial exopolysaccharides: Composition, structures, inducing factors and putative genes involved in their biosynthesis and assembly*, FEMS microbiology reviews, 33 (5) 917–941, 2009
- [6] A. Duro, V. Piccione, M. A. Ragusa, and V. Veneziano, *New environmentally sensitive patch index-ESPI-for medalus protoco*, In AIP Conference Proceedings, volume 1637, pages 305–312. American Institute of Physics, 2014.
- [7] H. Shen, L. Song, *Comparative studies on physiological responses to phosphorus in two phenotypes of bloom-forming Microcystis*, Hydrobiologia, 592 475–486, 2007.
- [8] Z. Yang, F. Kong, X. Shi, H. Cao, *Morphological response of Microcystis aeruginosa to grazing by different sorts of zooplankton*, Hydrobiologia, 63 225–230, 2006.
- [9] U. Sommer, E. Charalampous, M. Scotti, M. Moustaka-Gouni, *Big fish eat small fish: Implications for food chain length?*, Community Ecology , 9 107–115, 2018.
- [10] H. Malchow, S. Petrovskii, A. Medvinsky, *Pattern formation in models of plankton dynamics., A synthesis*, Oceanologica Acta, 24 (5) 479–487, 2001.
- [11] H. Yu, M. Zhao, Q. Wang, R. Agarwal, *focus on long-run sustainability of an impulsive switched eutrophication controlling system based upon the Zeya reservoir*, Journal of the Franklin Institute, 351 (1) 487–499, 2014.
- [12] D. Mukherjee, C. Maji, *Bifurcation analysis of a Holling type II predator-prey model with refuge*, Chinese Journal of Physics, 65 153–162, 2020.
- [13] B. K. Das, D. Sahoo, G. P. Samanta, *Impact of fear in a delay-induced predator–prey system with intraspecific competition within predator species*, Mathematics and Computers in Simulation, 191 134–156, 2022.
- [14] P. Akhtar, S. Karmakar, D. Sahoo, G. Samanta, *Dynamical analysis of a prey–predator model in toxic habitat with weak allee effect and additional food*, International Journal of Dynamics and Control, 12 (11) 3963–3986, 2024.
- [15] M. Hossain, S. Garai, S. Jafari, N. Pal, *Bifurcation, chaos, multistability, and organized structures in a predator–prey model with vigilance*, Chaos: An Interdisciplinary Journal of Nonlinear Science, 32 (6), 2022.
- [16] N. Pati, S. Garai, M. Hossain, G. Layek, N. Pal, *Fear induced multistability in a predator- prey mode*, International Journal of Bifurcation and Chaos , 31 (10) 2150150, 2021.
- [17] S. Sharma, G. P. Samanta, *Dynamical behaviour of a two prey and one predator system*, Differential Equations and Dynamical Systems, 22 (2) 125–145, 2014.
- [18] V. Piccione, M. A. Ragusa, V. Rapicavoli, and V. Veneziano, *Monitoring of a natural park through espi*, In AIP Conference Proceedings, volume 1978, page 140005. AIP Publishing LLC, 2018.
- [19] S. Saha, A. Maiti, and G. P. Samanta, *A michaelis–menten predator–prey model with strong allee effect and disease in prey incorporating prey refuge*, International Journal of Bifurcation and Chaos, 28(06):1850073, 2018.
- [20] B. Dubey, A. Kumar, A. P. Maiti, *Global stability and hopf-bifurcation of prey-predator system with two discrete delays including habitat complexity and prey refuge*, Communications in Nonlinear Science and Numerical Simulation, 67 528–554, 2019.
- [21] R. Banerjee, P. Das, D. Mukherjee, *Stability and permanence of a discrete-time two-prey one- predator system with holling type-iii functional response*, Chaos, Solitons Fractals, 117 240–248, 2018.

- [22] K. Chakraborty, S. S. Das, *Biological conservation of a prey–predator system incorporating constant prey refuge through provision of alternative food to predators: a theoretical study*, *Acta biotheoretica* , 62 183–205, 2014.
- [23] J. D. Murray, J. D. Murray, *Mathematical Biology: II: Spatial Models and Biomedical Applications*, Vol. 3, Springer, 2003.
- [24] B. K. Das, D. Sahoo, G. P. Samanta, *Fear and its carry-over effects in a delay-induced predator-prey model with additional food to predator*, *Filomat*, 37(18), 6059–6088, 2023.
- [25] L. Perko, *Differential Equations and Dynamical Systems*, Vol. 7, Springer Science and Business Media, 2013.
- [26] G. W. A. Nyakairu, C. B. Nagawa, J. Mbabazi, *Assessment of cyanobacteria toxins in freshwater fish: A case study of Murchison Bay (Lake Victoria) and Lake Mburo, Uganda*, *Toxicon*, 55 (5) 939–946, 2010.
- [27] Y. A. Kuznetsov, I. A. Kuznetsov, Y. Kuznetsov, *Elements of applied bifurcation theory*, Vol. 112, Springer, 1998.
- [28] S. Karmakar, P. Akhtar, D. Sahoo, G. Samanta, *Dynamical analysis of a predator-prey model in toxic environment with strong reproductive allee effect*, *Filomat* , 38 (10) 3597– 3626, 2024.